TECHNICAL UNIVERSITY OF LIBEREC
Faculty of Mechanical Engineering

Models for the prediction of cavitation aggressiveness

Master Thesis

Study programme:	N2301 Mechanical Engineering
Study branch:	Machines and Equipment Design
Author:	**Amila Džomba**
Thesis Supervisors:	Ing. Miloš Müller, Ph.D. Department of Power Engineering Equipment

Liberec 2021

TECHNICAL UNIVERSITY OF LIBEREC
Faculty of Mechanical Engineering

Master Thesis Assignment Form

Models for the prediction of cavitation aggressiveness

Name and surname: **Amila Džomba**
Identification number: S19000377
Study programme: N2301 Mechanical Engineering
Study branch: Machines and Equipment Design
Assigning department: Department of Power Engineering Equipment
Academic year: **2020/2021**

Rules for Elaboration:

Research on models used for the description of cavitation aggressiveness and cavitation erosion
Description of the material response to the cavitating flow impact
Analysis of available pitting tests and impact forces measurements
Preparation of a model for the description of interaction between the cavitating flow and the impacted material
Validation of the aggressiveness model on the available experimental data
Analysis of the model applicability for the cavitation aggressiveness prediction

Scope of Graphic Work: 10
Scope of Report: 50
Thesis Form: printed/electronic
Thesis Language: English

List of Specialised Literature:

FRANC, Jean-Pierre a Jean-Marie MICHEL. *Fundamentals of cavitation*. Dordrecht: Kluwer Academic Publishers, [2004]. Fluid mechanics and its applications, volume 76. ISBN 1-4020-2232-8.
BRENNEN, Christopher E. *Cavitation and bubble dynamics*. New York: Cambridge University Press, 2014. ISBN 9781107644762.
Kim, K. H., Chahine, G., Franc, J.-P. & Karimi, A. (2014) Advanced experimental and numerical techniques for cavitation erosion prediction. Dordrecht, Springer.

Thesis Supervisors: Ing. Miloš Müller, Ph.D.
Department of Power Engineering Equipment

Date of Thesis Assignment: November 1, 2020
Date of Thesis Submission: April 30, 2022

L.S.

prof. Dr. Ing. Petr Lenfeld
Dean

doc. Ing. Petra Dančová, Ph.D.
Head of Department

Liberec November 1, 2020

Declaration

I hereby certify, I, myself, have written my master thesis as an original and primary work using the literature listed below and consulting it with my thesis supervisor and my thesis counsellor.

I acknowledge that my bachelor master thesis is fully governed by Act No. 121/2000 Coll., the Copyright Act, in particular Article 60 – School Work.

I acknowledge that the Technical University of Liberec does not infringe my copyrights by using my master thesis for internal purposes of the Technical University of Liberec.

I am aware of my obligation to inform the Technical University of Liberec on having used or granted license to use the results of my master thesis; in such a case the Technical University of Liberec may require reimbursement of the costs incurred for creating the result up to their actual amount.

At the same time, I honestly declare that the text of the printed version of my master thesis is identical with the text of the electronic version uploaded into the IS/STAG.

I acknowledge that the Technical University of Liberec will make my master thesis public in accordance with paragraph 47b of Act No. 111/1998 Coll., on Higher Education Institutions and on Amendment to Other Acts (the Higher Education Act), as amended.

I am aware of the consequences which may under the Higher Education Act result from a breach of this declaration.

June 1, 2021 Amila Džomba

ACKNOWLEDGEMENTS

I have been extremely fortunate to have had the support of the department and family, near and far. First, I would like to express my deepest gratitude to my supervisor, Ing. Miloš Müller, Ph.D., whose knowledge and assistance cannot be overestimated. His expertise and understanding in the field of this study greatly improved content of this thesis and I thank him for guidance and constructive criticism. I would like to extend my sincere thanks to all the lecturers, academic staff and colleagues who have made a positive impact on me during these two years of my studies in Liberec. I am particularly thankful to the Ministry of Education, Youth and Sports of Czech Republic, for granting me a scholarship without which this journey would have been almost impossible.

I am deeply thankful to have Merim alongside at all times, grateful for his patience, never-ending encouragement, clever ideas and most importantly his constant appreciation and devotion.

Last but not least, I wish to thank my parents and my brother for believing in me, for their knowledge, unconditional love and lifelong precious advice.

ABSTRACT

The introduction to cavitation and its effects is described at the beginning of this study, as well as properties of fluid that affects cavitation and mechanisms of cavitation bubble collapse. Research on models which are used for cavitation aggressiveness and cavitation erosion description are studied. Further, description of material response to cavitating flow impacts with description of cavitation erosion is presented. Main stages, incubation, acceleration and steady state period, of cavitation are briefly described and focus is set on steady state period of cavitation. Existing pitting tests and impact forces measurements are taken into consideration and are utilized in this study. Experiment on vibratory apparatus is conducted in order to obtain mass loss data and erosion rate curve, as well as cumulative mass loss curve. Mass loss is measured until the steady state period of cavitation is reached since steady state period is the one of interest in this study. Results of the experiment are presented in the form of erosion rate graph and cumulative mass loss curve, since these are characteristic curves which describe cavitation erosion stages. Experimentally obtained erosion rate curve is compared to theoretical erosion rate curve and it is proven to be similar. Phenomenological model for cavitation erosion rate computation is studied and erosion tests are used in validation of the model. Applicability of the model on available experimental data is studied and results are presented. Results of experimental and analytical methods are compared and proven to be similar, of the same order. Conclusion is made that the experiments conducted in a couple of minutes are sufficient and there is a possibility to predict erosion rate based on these relatively simple experiments.

KEYWORDS: cavitation aggressiveness, cavitation erosion, phenomenological model, erosion rate, steady state period of cavitation

TABLE OF CONTENTS

LIST OF FIGURES

NOMENCLATURE

List of symbols

Roman letters

Symbol	Name	Unit
A	Parameter used in equation for stress pulse distribution	-
d	Diameter, or single-damage size	m
d_m	Average value of single-damage size	m
$\dot{E}$	Erosion rate during steady state period	kg/s
$\dot{e}$	Erosion rate during acceleration period	kg/s
g_{33}	Piezo stress constant	$V/m \ / \ N/m^2$
$h(t)$	Total eroded depth after exposure time t	m
K	Strength coefficient	MPa
L	Maximum depth of hardened layer of eroded material	m
l	Depth of hardened layer	m
ΔL	Length of rupture due to one cycle of impacts	m
ΔL_m	Average value of length of rupture	m
m	Mass	kg
n	Work hardening coefficient	-
N	Total number of impacts	$count$
N_h	Ratio of number of impacts	-
N_p	Number of impacts which contribute to material loss	$count$
N_s	Number of impacts distributed over the surface	$count$
$\dot{N}$	Rate of impacts	$count/s$
$p_B(t)$	Pressure within the bubble	Pa
$P(d)$	Probability density function of size distribution	-
p_{GM}	Partial pressure of gas	Pa
p_v	Saturated vapor pressure	Pa
p_∞	Reference pressure	Pa
$P(\sigma)$	Probability density function of stress pulse amplitudes	-
$P(\sigma_U)$	Probability density function of ultimate stress amplitudes	-
R_i	Measured value of radius	m
r_i	Indentation radius, real value	m
R_m	Maximum radius of a bubble	m
R_0	Original nuclei size	m

$R(t)$	Instantaneous bubble radius	m
S	Surface tension	N/m
S_m	Average area of impacts	m^2
S_0	Exposed area	m^2
t	Time	s
T_c	Critical point temperature	°C
t_{PVDF}	Thickness of PVDF film	m
T_r	Triple point temperature	°C
U_∞	Reference velocity	m/s
v	Volume	m^3

Greek letters

Symbol	Name	Unit
α	Shape parameter in the stress pulse distribution	-
β	Scale parameter	-
ε	Strain	-
ε_R	Rupture strain	-
$\Delta\varepsilon_x$	Strain increment at distance x from the impacted point	-
$\Delta\varepsilon_0$	Strain increment at the impacted point	-
θ	Internal strain hardening parameter of material	-
μ	Parameter used in equation for size distribution	-
ν_L	Liquid kinematic viscosity	m^2/s
ρ	Density of eroding material	kg/m^3
ρ_L	Density of liquid	kg/m^3
σ	Stress	MPa
σ_a	Stress pulse amplitude of cavitation collapse	MPa
σ_{am}	Mean stress pulse amplitude beyond ultimate stress	MPa
σ_{ca}	Cavitation number	-
σ_U	Ultimate strength (stress)	MPa
σ_Y	Yield strength (stress)	MPa
ω	Shape parameter in the size distribution	-

List of abbreviations

ASTM	American Society for Testing and Materials
BEM	Boundary Element Method
ICET	International Cavitation Erosion Test
PVDF	Polyvinylidene Fluoride
SEM	Scanning Electron Microscope

1 Introduction to cavitation

Cavitation begins with the formation of cavitation nuclei. When a liquid is subjected to a certain pressure below its vapor pressure, at a certain temperature, it can be said that the liquid is under tension, and cavitation occurs. It is also valid that cavitation is the formation of bubbles resulting from depressurization or lowering the pressure at a certain constant temperature and it occurs in the body of a liquid [1]. There can be various forms of weaknesses in the liquids that lower the achievable tension of liquid itself, and all of those forms of weaknesses yield a different vapor bubble formation process. Vapor bubble formation process in which presence of small, temporary gaps between molecules is caused by random thermal motions of the molecules is called homogeneous nucleation. When there is a contact between a liquid and a solid, another kind of nucleation can occur on the interface between a solid and a liquid, and it is called heterogeneous nucleation. A liquid can also contain minor gas bubbles, so-called microbubbles usually stabilized by surface tension effects, but they can become macroscopic bubbles under adequate amount of tension. Lastly, weakness in a liquid can be caused by radiation from the outer surface [1]. As mentioned before, the process of cavitation occurs due to depressurization at a relatively constant temperature, which can be shown in a phase diagram, visible in Figure 1. Prediction of formation and control of nucleation sites is unsure even when dealing with liquids as common as water [1].

To determine the potential for cavitation phenomena we use the term cavitation number σ_{ca}, which tells us how close the pressure of the liquid is to the vapor pressure. It is described with the equation 1,

$$\sigma_{ca} = \frac{p_\infty - p_V}{\frac{1}{2} \cdot \rho_L \cdot U_\infty^2} \qquad 1$$

where p_∞ is reference pressure, p_V (T_∞) is saturated vapor pressure, T_∞ is reference temperature, ρ_L is the liquid density and U_∞ is reference velocity [2]. It is noticeable that cavitation number, σ_{ca}, is defined using dynamical parameters and not geometrical ones. If the value of cavitation number is high, there would not be a presence of cavitation, the cavitation would be absent, or there would be a very slight change of cavitation existence. If the value of cavitation number is low, the

cavitation would be present and for the even lower values the cavitation would be more developed [2]. With this said, cavitation number is used as an indicator of the development or the extent of the cavitation in a liquid flow. When the velocity is increased at a constant cavitation number, the ambient pressure must be increased as well in order to conserve the cavitation number, but this results in bubbles experiencing larger pressure and a stronger bubble collapse [2].

The growth and collapse of a bubble is governed by Rayleigh-Plesset equation, equation 2, which connects the instantaneous bubble radius to the prevailing pressure away from the bubble,

$$\frac{p_B(t) - p_\infty(t)}{\rho_L} = R\frac{d^2R}{dt^2} + \frac{3}{2}\left(\frac{dR}{dt}\right)^2 + \frac{4 \cdot \nu_L}{R}\frac{dR}{dt} + \frac{2 \cdot S}{\rho_L \cdot R} \qquad 2$$

where $R(t)$ is instantaneous bubble radius, $p_\infty(t)$ is prevailing pressure, $p_B(t)$ is pressure within the bubble, ν_L is the liquid kinematic viscosity and S is the surface tension [1]. Equation 2 is used under the assumption that no significant temperature differences were generated in a liquid during the growth of a bubble, and that the bubble is spherical in shape. Bubble growth is fairly steady but the collapse of a bubble is often immediate and catastrophic. Whatever the initial size, all activated nuclei grow roughly the same maximum size, and all the bubbles in a cavitating flow tend to grow to approximately the same size no matter what the initial nuclei size is [1]. In liquids other than water or at higher temperatures, temperature differences develop between the volume of the liquid and the vapor/liquid interface which significantly change and slow down the growth rate. This is termed as thermal effect and by slowing down the growth rate of a bubble it reduces unfavorable effects of cavitation [1].

Vapor or cavitation bubble collapse in the absence of thermal effects can lead to considerable interface velocities as well as considerable localized pressures. Cavitation bubble collapse can damage nearby surfaces in critical ways. Analysis in which it is assumed that a bubble remains spherical provides a convenient starting point. Collapse of a bubble will begin at its maximum radius, R_m, as it grows from a small nucleus to a bubble which is far greater than the original size of nucleus, and the collapse will happen with considerably small partial pressure of gas. A maximum size of a collapsing bubble, in a typical situation of cavitating flow, is 100 times larger

than the original nuclei size, and the value of pressure of gas is considerably small at the beginning of bubble collapse. Temperature is also worth mentioning as it can rise up to the maximum value of $4 \cdot 10^4$ times the ambient temperature. As the bubble collapses, it is clear that there is a potential for generating high pressures and temperatures but also the potential for the generation of noise and shock waves. Shock waves can occur in a rebound phase, which is a phase right after the bubble collapse happens. The time between the bubble growth phase and bubble collapse phase is in the order of microseconds, and it is safe to say that during that time the gas in the bubble behaves adiabatically. Even though this phenomenon of bubble collapse happens rapidly, it is capable of producing fascinating effects such as sonoluminescence or flashes of light during the collapse [1].

During the last stage of bubble collapse the bubble is most unstable to non-spherical disturbances. There are several different outcomes to this. First of the possibilities is such that the bubble surroundings are a solid boundary or a free surface, and in these two cases we can expect outcome in the form of re-entrant jet. Cavitating bubble collapse near a solid boundary can cause a re-entrant microjet directed toward the boundary. When the cavitating bubble collapses near a free surface it produces the re-entrant microjet directed away from the surface. Which microjet will appear, toward or away from the surface, depends also on flexibility of the surface itself [1]. That is the reason why some metals are covered or painted with a layer of coating with high flexibility. Another possible outcome is the proximity of other cavitating bubbles and formation of finite clouds of bubbles. In this case, bubbles on the outer edge of a bubble cloud will tend to develop microjets directed to the inside of the cloud itself.

When the cavitation bubbles collapse near the solid surface they can seriously damage the material, and that is the global and inescapable engineering problem. This problem is complicated because it involves the unsteady flow phenomenon and the reaction of the particular kind of material of which the solid surface is made. Since cavitation bubble collapse is a damaging and violent process which yields microjets and shockwaves, the appearance of surface stresses is not surprising. With the cavitation bubble collapse comes the cavitation noise, and that noise happens instantly when the bubble is highly compressed. The crackling noise which comes

along with cavitation is usually one of the most evident characteristics of this phenomenon and the first sign of cavitation could be detected by the sound observation rather than visual observation of cavitation bubbles.

1.1 Classification of cavitation

Cavitation occurs when the pressure of the liquid drops below the vapor pressure of that same liquid. Figure 1 represents the phase diagram of water. Description of cavitation is illustrated in the phase diagram.

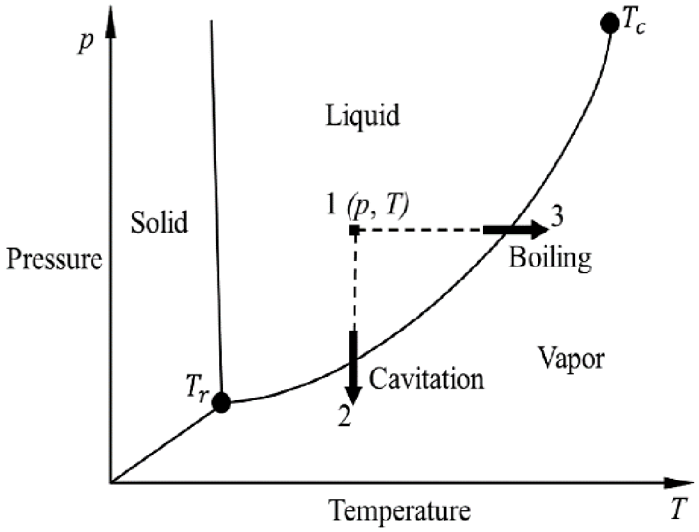

Figure 1 - Phase diagram of water;
T_r represents temperature corresponding to triple point
and T_c temperature corresponding to critical point [10]

There are different types of cavitation which can occur. Common phenomenon which frequently occurs along hydrodynamic machinery, such as pumps, propellers, turbines or valves, is named hydrodynamic cavitation [3]. It arises as a result of rapid pressure drop or a reduction in pressure of flowing liquid due to geometry of previously mentioned machinery, where it is known that the acceleration of the flow exists. This type of cavitation is characterized by the fact that pressure drops are caused by increases in the average velocity field. Cavitation can also exist in a nearly static liquid. Example of this is when a solid body with sharp edges starts to accelerate rapidly, thus creating cavitation bubbles. Type of cavitation which can be formed by ultrasonic waves in a liquid is known as acoustic cavitation [2]. Phenomenon which occurs in this type of cavitation is closely connected to a growth

of preexisting cavitation microbubbles under the influence of ultrasonic field. Emission of light from this cavitation type – sonoluminescence, and the intensity and its spectra are altered when cavitation is induced at different frequencies [4].

1.2 Effects of cavitation

Depending on the application, cavitation can either have useful or detrimental effect when the bubbles eventually collapse near a solid surface. Formation of bubbles in any liquid medium can create unstable regions which, as a result, causes reduction in pressure leading to collapse of a bubble. When it comes to hydraulic systems, impact of cavitation produces undesirable effects which highly alter the performance of the systems and their performance, and also reduces their efficiency. Some of the undesirable effects which collapse of cavitation bubble produces are deterioration of hydraulic equipment, damage from pit formation, erosion of the solid body, mechanical vibrations and even noise caused by structural damage [5]. If the cavitation bubble collapse happens repeatedly near a solid surface, it can cause fatigue failure as well as total damage of material in hydraulic machinery. In the places where high velocities are expected, unfavorable cavitation damage can be expected as well. In order to have hydraulic systems operating at their highest efficiency, it is necessary to consider the impact of cavitation when designing the systems or equipment.

However, not all bubble collapses have detrimental effect. Acoustic cavitation has found its use in biomedicine, as a localized drug delivery system [6]. In medical field, cavitation brings fortunate result for special surgical procedures. Positive use of cavitation is also noticeable in cleaning applications in the form of ultrasonic cavitation, where the implosion of a bubble contributes to the removal of contaminants from the surface without damaging it [5]. Cavitation phenomena and the collapse of a cavitating bubbles has found its use in many different fields.

1.3 Properties of fluid affecting cavitation

Several physical properties can influence the cavitation phenomenon, each in its own different way. When there is high surface tension of the liquid, the lower the pressure is needed for cavitation, and growth of the bubble is slowed down.

Also, higher surface tension drives the conclusion that it has an anti-cavitation effect. This is the influence of surface tension of liquid. If the viscosity of a fluid increases, the velocity of the fluid decreases and also its pressure decreases, and cavitation inception conditions worsen. This is the influence of fluid viscosity [3]. Air content in the bubble is also important for cavitation. If the bubble has large air content thus large initial radius, greater cavitation pressure is needed. Therefore, it is easier to achieve cavitation when the core of the cavitation bubble is larger. This is the influence of air content [3]. Only some properties affecting the cavitation are listed above, as there are many more.

1.4 Mechanisms of cavitation bubble collapse

Asymmetry in the form of nearby solid surface, or simply a wall, is taken into account, and mutual effect of the wall and the bubble collapse near the solid boundary is observed further.

1.4.1 Collapse of a single bubble

Bubble collapse is crucial subject because of the material damage and noise that can be caused by the high velocities, pressures and temperatures that arise from the collapse. It is assumed that a bubble remains spherical. Normally, collapsing bubbles do not maintain their spherical shape and they are sometimes far from spherical. However, maximum possible consequences of bubble collapse in terms of the damage potential, noise or temperature are obtained when the analysis is conducted with the assumption that the bubble is spherical in shape. Collapse of a bubble will begin at a maximum radius of a bubble, R_m, with a very small partial pressure of gas, p_{GM}. In a typical cavitating flow, R_m is of the order of 100 times the original nuclei size, R_o [1]. As the implosion of bubble occurs, the bubble is compressed. There is a limit up to which the bubble can be compressed to its maximum, because of the vapor volume inside the bubble.

A bubble can rebound a few times after the collapse and in this rebound phase, bubble is highly distorted. In Figure 2, bubble rebound can be observed. During the collapse there is a great potential for the generation of high pressures and temperatures as well as potential for generation of shock waves and noise [7].

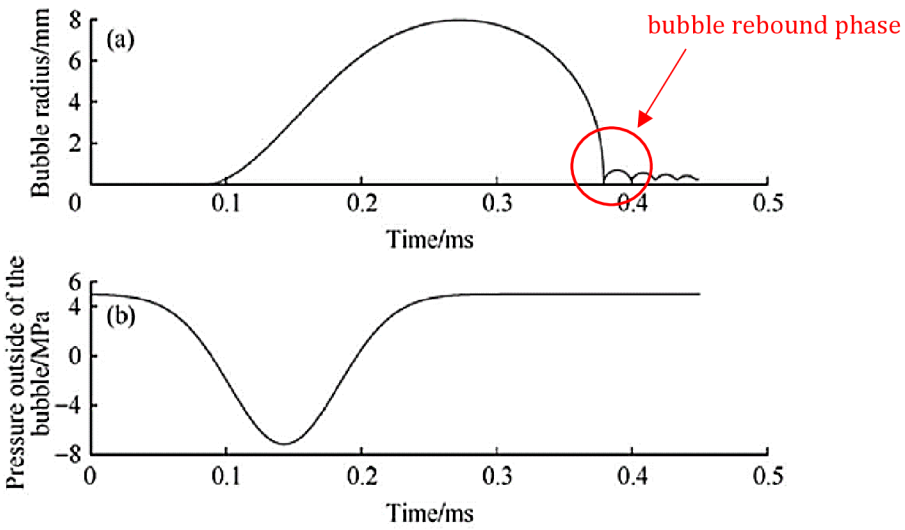

Figure 2 – Variation of bubble radius (a) and corresponding pressure value outside of the bubble (b) with time [36]

1.4.2 Cavitating microjet

Dominant phenomenon in the collapse of many cavitating vapor bubbles is the development of the re-entrant cavitating microjet due to asymmetry in the form of presence of nearby solid surface [8]. This asymmetry, in the form of solid surface, is known to cause one side of the bubble to accelerate inward more rapidly than the opposite side. As an effect, this can cause high-speed narrow beam of liquid or a microjet which penetrates the bubble, during its non-symmetrical collapse. In other words, the narrow beam of liquid goes through the bubble itself and makes a gap, and the bubble can obtain a shape of a torus [9]. Microjet is referred to as a jet forming on the bubble wall and moving across the bubble interior, before piercing

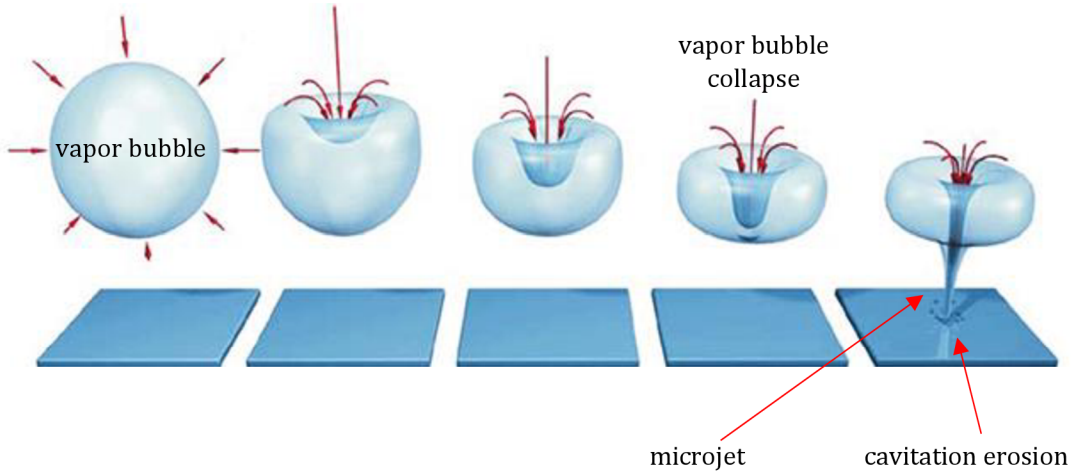

Figure 3 - Formation of cavitating microjet [37]

the wall on the opposite side. This microjet has a very high velocity and with that, high energy. Microjet formation can be observed in Figure 3. At the impact point or at multiple points where the microjet occurs, there is a significant increase of temperature and pressure, in the form of pressure waves, and even noise. There are situations when it is difficult to observe the microjet. One of them is when the initial bubble is relatively close to a solid surface and the bubble collapse begins from a spherical cap shape and it "pancakes" down toward the surface [7]. Sometimes other asymmetries, such as gravity, can also cause a re-entrant microjet formation.

1.4.3 Jet shock wave and collapse shock wave

Shock waves are one of the most destructive phenomena which can occur during the collapse of a cavitation bubble. Cavitation bubble collapse is a violent process that generates highly localized, large-amplitude shock waves and microjets in the fluid at the point of the collapse [7]. After the disturbance caused by cavitating microjet, a cloud of small bubbles - which continue to collapse collectively, are left as residue. Even though this is not just one single bubble but many small bubbles or cloud of small bubbles, they will still show the same bubble dynamic behavior, including the possible creation of shock waves [7]. Before the bubble hits the solid boundary, as the cavitating microjet pierces the bubble, a shock wave named jet shock wave is generated [10]. The occurrence of multiple shock waves during the bubble collapse is expected. As the first jet shock wave appears, another shock wave comes right after the bubble collapse and that shock wave is called collapse shock wave. Collapse shock wave occurs due to high compression of the gas bubble [10]. Intensity of the shock waves depends on the mutual closeness of the bubble and solid boundary, and it increases when the bubbles collapse at a shorter distance to the solid boundary. Sphericity of a bubble near a solid boundary has a great effect on the strength of a collapse shock wave. Most energetic shock waves are emitted by the collapses of bubbles which are in shape of almost perfect sphere. Gasses inside the bubble are compressed rapidly and with the compression comes rise in temperature and those temperatures can reach levels of visible light emission, phenomenon known as luminescence [11]. Shock wave generated as the cavitation bubble collapses strikes the material surface and the impact energy causes plastic

deformation which changes the residual stress. Various phenomena occurring during cavitation erosion process is presented in Figure 4.

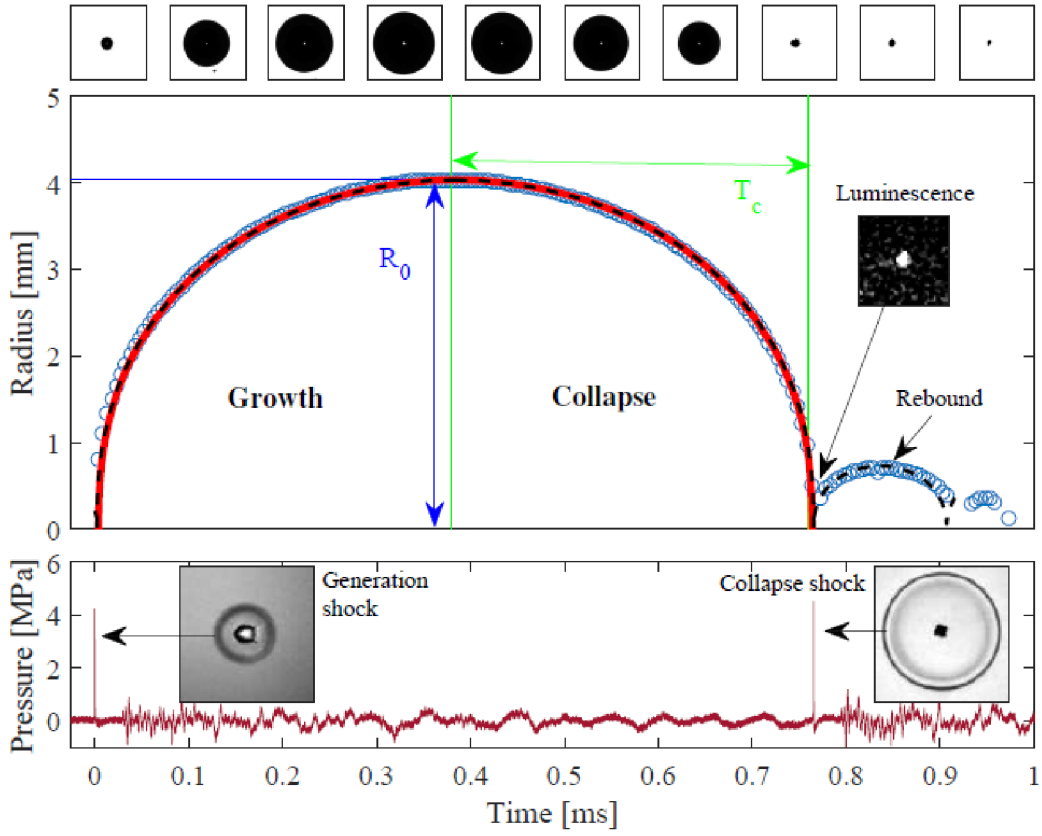

Figure 4 – Multiple phenomena presented, with collapse shock wave in the bottom of the figure. Top of the figure: shadowgraph visualization of spherical bubble growth and collapse, middle: evolution of a bubble, bottom: pressure signal as a function of time [11]

Cavitating microjet and bubble collapse shock wave are two of the most observed phenomena which take place during the bubble collapse. There are others which also appear, but are harder to observe since they occur more rapidly than two aforementioned. They take place between the appearance of microjet and shock wave. One of them is vapor torus. After the initial bubble collapse, the bubble forms a torus shape which then divides into other smaller bubbles which collapse subsequently [12]. Toroidal cavity is also worth mentioning. It occurs after the impact of the cavitating microjet. Toroidal cavity acts as a force on the nearby solid

boundary and that causes so-called splash effect [5]. Some studies suggest that this splash effect induced by the effect of toroidal cavity can produce a higher hydrodynamic pressure on the nearby solid surface than the pressure produced by the cavitating microjet [13]. Development of the splash effect is dependent on the thickness of the liquid layer between the bubble and the solid boundary.

1.5 Material response to impact loads

In case of cavitating bubble collapse near a solid boundary, disturbances like microjets and shock waves generate surface stresses. Repetition of these disruptions with repeated bubble collapses induces surface fatigue failure and the subsequent detachment or flaking of pieces of material [7]. Independent of the loading mechanisms, some of which are described above, the material exposed to cavitation can experience high intensity, short duration pressure pulses which induce plastic deformation in the layers under the surface and produce permanent pits on the material surface. Mechanical properties of most engineering materials used vary with the strain rate. Figure 5 illustrates examples of the influence of strain rate on the flow stress of different alloys, where the flow stress is an instantaneous stress to sustain plastic deformation at a particular strain [2].

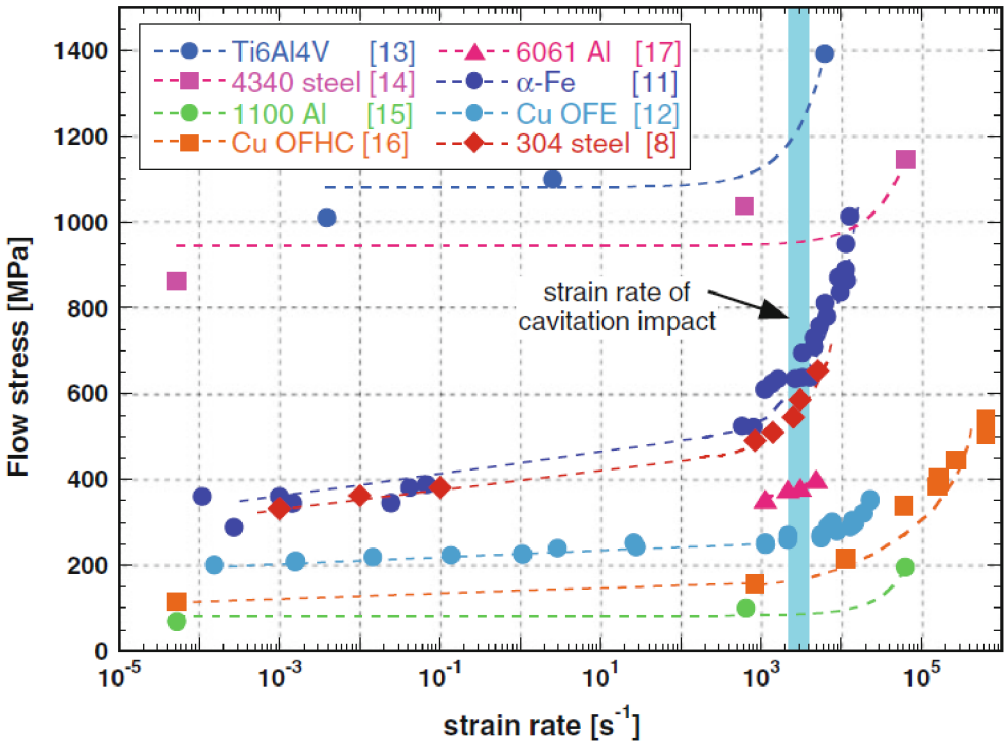

Figure 5 – Influence of strain rate on flow stress of different alloys [2]

1.6 Cavitation erosion

Bubble collapse adjacent to a solid boundary results in pitting or erosion of the material surface, or component failure in the long run. Cavitation erosion is considered to be steady material damage induced by repeated impulsive loads in the form of microjets and/or shock waves, which are known to be created by collapsing cavitation bubbles [2]. Repetitive loading causes fatigue which is notably obvious during incubation period since cavitation bubbles collapse repetitively on the material surface without producing any mass loss. This phenomenon of cavitation erosion occurs in various stages, starting from an initial incubation period, followed by acceleration, deceleration and in the end steady state period. Material surface undergoes plastic deformation, progressively moving to material damage and failure, as well as material mass loss due to repeated cavitation impact loads [2]. All stages of cavitation erosion are presented in Figure 6.

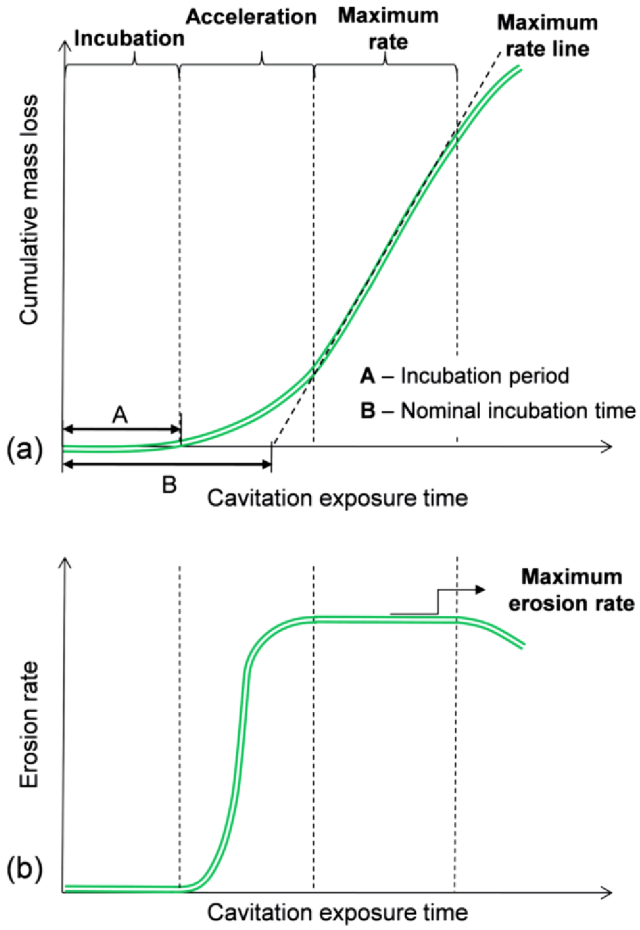

Figure 6 - Characteristic curves of cumulative mass loss and erosion rate vs. cavitation exposure time [35]

1.6.1 Incubation period

Initial stage of cavitation erosion is known as incubation period. During this stage there is insignificant mass loss and the damage by erosion is characterized by localized indentation, called pits. Idealized cavitation pit is presented in Figure 7.

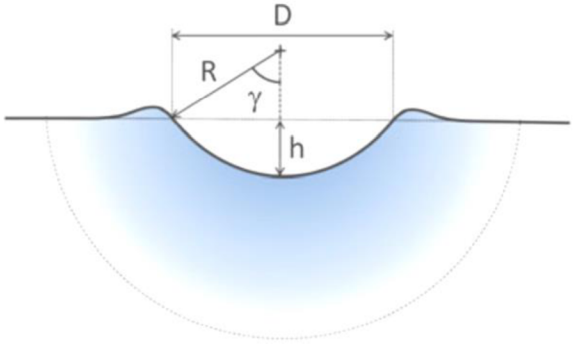

Figure 7 - Sketch showing idealized cavitation pit; blue shape around the pit is described as plastic zone [2]

Pits are known as plastic, small deformations, approximately circular in shape. They are visible in cases when the material's surface is finely polished, as they can be of similar elevation as surface roughness. Pits are scattered if the exposure time to the cavitation is small. As this time increases number of collapses of cavitation bubbles increases as well and with this the number of pits progressively overlap and the surface of the material becomes more and more deformed and it hardens [2]. If the exposure time is even more increased, the material surface becomes covered by cavitation impacts several times and more severe damage takes place, including material failure. During the incubation period, cumulated plastic strain progressively increases until material damage and finally failure occurs. When the material damage occurs, it is a sign that the incubation period has ended and the acceleration period, or mass loss period has begun. Each pit is considered to be created by single cavitation event generating an impact load exceeding the material yield strength [10]. During incubation period, microjets and shock waves are hitting the material surface but there is no erosion. However, there are some permanent deformations. To characterize the aggressiveness of cavitation flow, pitting tests are often used.

Connection of stress-strain curve and incubation period

A connection between the stress-strain curve (σ-ε curve) and incubation period can be made. Firstly, the yield strength of the material is an important constant. The stress level where the material starts to strain plastically is termed as the yield stress. When any material is stressed by any amount that is less than the material's yield stress it will only undergo elastic strain, and no permanent deformation will occur [2]. The level of stress that corresponds to the yield stress is known as yield strength of the material [14]. As noted before, it is a constant for each material. Stress-strain curve is presented in Figure 8.

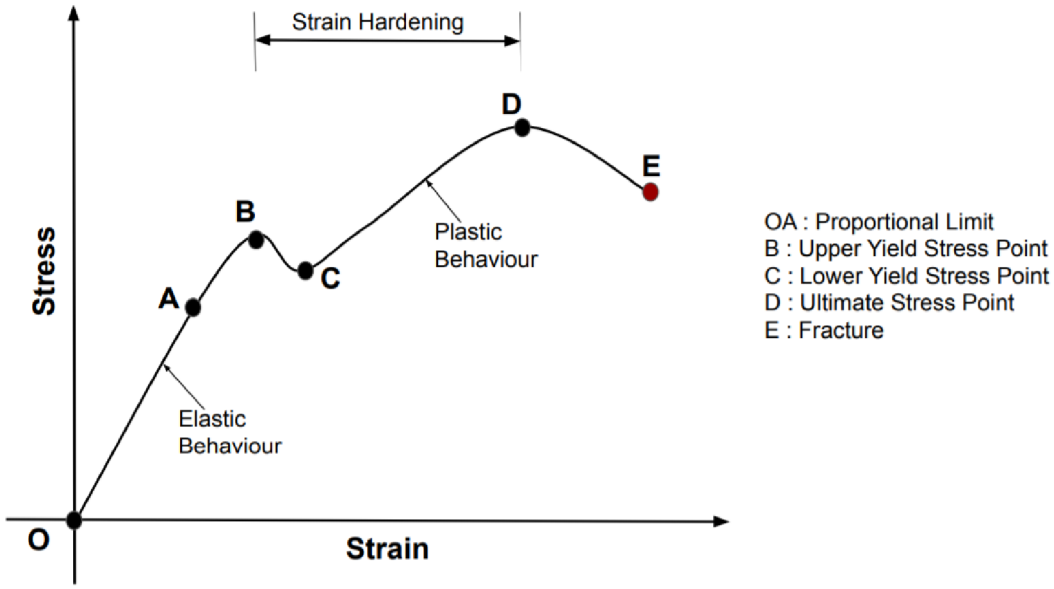

Figure 8 - Stress-strain curve [34]

During the incubation period we can observe and go along the σ-ε curve. At the beginning of every said curve there is elastic deformation period. In this part of the curve, cavitating microjet hits the material surface and if the force given by the cavitating microjet does not overcome the limit given by material's yield strength, there is no permanent deformation. Still, the elastic part of the σ-ε curve is observed. At one moment, yield strength of the material would be reached and after reaching yield strength permanent plastic deformation can be observed [10]. Even though there are permanent deformations, there is still no mass loss. Fracture point on any σ-ε curve is an area where the incubation period ends. Fracture point means the strength limit of the material has been reached and mass loss occurs past this point. Period which follows the incubation period – acceleration period is reached by reaching the fracture point along the σ-ε curve.

Another phenomenon can be observed amid the incubation period and it is named strain hardening. Strain hardening occurs with the increase of velocity of the impact of microjet. It is the strengthening of material by plastic deformation, or simply put, it makes material stronger [15]. Response of a material under cavitation impact could be compared to random cycle fatigue. Cavitation erosion can be considered a special type of fatigue phenomenon since the frequency of impacts is usually very high and the magnitude is very random, which leads to local stress in the material itself which can vary in wide range from elastic to plastic domain. Impact loads vary, with random intervals, magnitudes and random locations of impact on the surface.

Strain rate sensitivity of the material

Flow stress, also called ultimate or tensile strength is the stress that must be applied to cause a material to deform at a constant strain rate in its plastic range [16]. It is the instantaneous value of stress required to continue plastically deforming the material, or to keep the metal flowing. On a stress-strain diagram, flow stress is observed from the yield point, including the yield point and to the fracture point, excluding the fracture point. This part of the curve deals with the plastic deformation or the plastic flow of the material. At hot working temperatures flow stress depends on strain rate. As the strain rate increases the resistance of the material to deformation increases as well. This effect is known as strain rate sensitivity.

To further explain strain rate sensitivity of the material a written example is presented [17]. In the example, two cases are observed. In the first case, material is loaded fast and one σ-ε curve is obtained. In the second case, the same material is loaded slowly and different σ-ε curve is obtained. If the curves would be different for the first and the second case then the material is considered to be strain rate sensitive. On the other hand, if the σ-ε curves are the same for the first and the second case then the material is considered not strain rate sensitive. Strain rate sensitive simply means a material's σ-ε characteristics are dependent on the rate of the loading of the material.

Residual stress

Generally speaking, residual stress is the internal stress distribution locked into a material. This stress is present even after all external loading forces are removed [18]. Mechanical, thermal or processes which include phase change can cause residual stresses. As mentioned before, cavitation can have positive and negative effects when it occurs. It can cause vibration, noise, reduction in performance and erosion in pumps, turbines or ship propellers. On the more positive note, cavitation can be applied to apparatus for sterilization, purification, material cutting and material modification as work hardening and residual stress improvement [19]. Residual stress of a material can be improved by various surface enhancement techniques. One of the surface enhancement techniques is cavitation shotless peening, which makes use of cavitation impact to induce compressive residual stress

on the metallic materials. This increases fatigue life of components [19]. Another technique is shot peening, which is used to prevent the cracking of the materials. By shot peening, shot material is enlarged and if there are any imperfections, scratches or flaws that are underneath that surface they become hidden under the pits on the top, and therefore they cannot open up and cause the said material to fail. When the material is peened, residual stress changes from tensile to compressive [20]. Compressive residual stress is a measurement of tension of the surface of the material. This stress limits the existence of stress corrosion cracking on the weld surface, for example. It is induced at the surface by the breach of the shot, effectively cold working it through plastic deformation, with visible series of overlapping pits. High compressive stresses make the fatigue crack formation more difficult and slow down the fatigue crack growth, and in this way improves the cavitation erosion resistance [21]. Cavitation erosion and residual stress of a material are both very closely connected to plastic deformation. As the cavitation bubble collapse occurs, shock wave hits the material and the energy of the impact causes the change in residual stress, and causes plastic deformation [2].

1.6.2 Acceleration period

As the exposure time increases the pits start to overlap leading to rapid depletion called acceleration period. Duration of the acceleration period is the time required to reach the steady state period and it is the sum of the coverage times until the end of acceleration period. Transition from incubation to acceleration period is defined with the start of cavitation erosion. Mass loss occurs during this stage and it increases with the exposure time.

1.6.3 Steady state period

Steady state period is characterized by constant mass loss over certain exposure time and it follows acceleration period [12]. Strain profile inside the eroded material also remains constant. Constant number of impacts per unit time and unit surface area is considered for a steady state period of cavitation.

2 Research on models used for the description of cavitation aggressiveness and cavitation erosion

Numerical modeling and simulation of the non-spherical dynamics of bubble near rigid and deformable boundaries with known material elasto-plastic properties are presented as well as examination of response of the material to the loads generated by a bubble collapse. Each of the various parameters, such as bubble size, distance from the wall and material properties, can be isolated and its influence on the spatial and temporal distribution of impulsive pressures resulting from the bubble dynamics, and on material elasto-plastic deformations in response to these loads can be observed [22].

2.1 Numerical models

Numerical simulation can be done on cavitating flow field, bubble dynamics and dynamic material response. It is done using several numerical methods, these include:

- 3DYNAFS-BEM – a boundary element method potential flow model for 3D bubble dynamics
- GEMINI – a finite difference method compressible Euler flow solver, for bubble dynamics
- a procedure to link incompressible-compressible flow approaches
- DYNA3D – a finite element structural dynamic code, to model material and structural response [22].

2.1.1 Flow field models

Boundary element model – 3DYNAFS-BEM

This model is based on the Boundary Element Method (BEM) and it uses Green's theorem to reduce the number of dimensions of the problem by one [23]. A flow problem in a 3D domain can be solved by the discretization of the surfaces which surround the flow domain. Using this method, a severe cut in computational time compared to other volume-based fluid dynamic codes is achievable. This method was developed specifically to solve 3D potential flow problems including highly

non-linear free surface dynamics which can be experienced in bubble dynamics and ocean dynamics. 3DYNAFS-BEM can be connected with DYNA3D which is a structural code, for simulation of fluid-structure interaction problems [22].

Compressible flow model – GEMINI

GEMINI is based on a finite difference scheme. It is a compressible Euler equation solver. GEMINI code applies a high order Godunov-type method and can accurately capture the location of discontinuities in the form of shock waves and contact surfaces. This model can be connected with a structural code in order to anticipate the response of a nearby structure. It can also be linked to 3DYNAFS-BEM to model various stages of bubble collapse efficiently and accurately [22].

Incompressible-compressible link procedure

BEM can accurately describe re-entrant jet formation and provide characteristics of a jet as a function of time since re-entrant jet velocity or bubble wall velocities are small relative to the speed of sound in water until the final stage of bubble collapse. Cavitation bubble collapse modeling near the boundary has been done using potential flow boundary methods. During the bubble growth, rebound and jet impact, there are non-negligible compressible effects. Compressible approach is needed in a case where these phenomena occur, since they may lead to wave creation and propagation. BEM is efficient in reducing the dimension of the problem by one, i.e. 2D problem (axisymmetric) becomes 1D problem involving line integrals, 3D problem is reduced to surface integrals enclosing the 3D domain. With reduction of dimension, very fine gridding is possible which increases accuracy with reasonable computation time. Aforementioned 3DYNAFS-BEM has been shown to provide re-entrant jet parameters precisely but it does not work well on computations beyond the surface impact, i.e. when re-entrant jet hits nearby solid wall in the case of liquid-solid impact [22].

Compressible finite element models, e.g. GEMINI Euler equation solver, are most appropriate to model shock wave emission and propagation. Compared to BEM, these methods require very fine grids and small steps to resolve shock wave fronts. Compressible model like GEMINI is most appropriate to model the shock wave propagation stage only [22].

A hybrid method takes advantage of strengths of both the BEM and compressible Euler methods. It was developed at DYNAFLOW and it addresses underwater explosion bubble problems and is used for cavitation erosion bubble dynamics problems. Principle of the method is such that geometry, grids and flow information are exchanged between the two methods, BEM – as the incompressible, and compressible whenever needed. Information exchanged between the two is called a *link*. This link makes sure that one method can pursue the problem resolution starting from the solution given by the other method. GEMINI is used during the impact or during the shock formation stage on the materials and the 3DYNAFS-BEM is used during most of bubble dynamics where the liquid velocities are very small compared to speed of sound [22].

2.1.2 Structural model

Example of a non-linear explicit solid and structural dynamics solver based on finite element method is DYNA3D. This model is appropriate for problems where high strain rate dynamics of stress wave propagation effects are important. Wide range of material behavior, including elasticity, plasticity, damage, failure and thermal effects, is represented by many material models [22].

3 Description of the material response to the cavitating flow impact

3.1 Brief description of phenomenological model of erosion

When predicting cavitation erosion, most of the work is limited to providing correlation functions between erosion rate and material properties of a material obtained by conventional mechanical testing. Analytical erosion model is proposed as opposed to the aforementioned models [24]. This model describes erosion rate as a function of cavitation loading and material response [25]. Model takes into the account deformation processes and failure mechanisms which take place under cavitation loading. During cavitation erosion it is assumed that a material is exposed to repeated impulsive loading. Amplitude, frequency and distribution of the impulsive loading over the exposed area is determined by the flow conditions. These impulsive loads can induce local deformation in the subsurface layers at high strain rates and create different shaped pits. Near surface layers progressively harden with the accumulation of local strains. When the overall plastic strain of the surface layers reaches the fracture limit of the material, cracks propagate through the subsurface layers leading to material erosion. In the early stage of erosion, topography of the eroded surface consists primarily of small pits and tear type ruptures with micro voids. As the erosion advances, surface roughness becomes more noticeable leading to the formation of typical hill and valley morphology with large scale irregularities and holes [24].

3.1.1 Material deformation

Failure of materials under compressive stress can be different from its failure under tensile stress. Use of tensile parameters is explained by the fact that compressive strength of materials is less documented compared to the tensile strength. However, in metallic materials there is no significant difference between the compressive and tensile values. Erosion rate of the material will depend on the stress-strain relation of the material and on the flow aggressiveness, i.e. rate, intensity and distribution of impulsive loads. Total deformation of the eroding sample is the accumulation of single impact strains [24].

3.1.2 Cavitation aggressiveness

Cavitation aggressiveness is characterized by statistical distribution of impacts in terms of frequency, intensity and size [24]. Considering radial extent of the load, it is assumed that the surface area of the loads is correctly characterized by mean surface area even though the loads are distributed over certain range of diameters. Cavitation aggressiveness is expressed with a probability density function of impacts. Using a curve fitting method, distribution type which works with the probability density function is found. There are two categories of impacts which can be divided with respect to the ultimate strength of material, σ_U. Impacts with amplitude smaller than σ_U contribute only to work hardening and fatigue, and impacts with amplitude higher than σ_U can create fracture and generate erosion in addition to plastic deformation. With this presumption, number of impacts directly involved in erosion, with respect to time, is defined as total number of impacts whose amplitude is greater than material's ultimate strength, σ_U. As erosive amplitudes have various values, mean value of amplitudes beyond the ultimate strength of material will be characterized in the model [24].

3.2 Main principle of erosion rate computation model

The model advances by time steps corresponding to the repeated coverage of material surface by cavitation impacts [24]. At the beginning, damaging impacts are all the impacts whose amplitude is greater than the yield stress, σ_Y. Principle of the erosion rate computation is presented in Figure 9.

Using stress-strain curve, a value for ε_1 can be found, as it corresponds to σ_1 value. As the first coverage comes to an end, strain will have a value of ε_1 on the entire material surface. During the first coverage, material flow stress increases from yield stress, σ_Y to σ_1. Second coverage involves only cavitation impacts with amplitudes higher than σ_1. After calculation of first coverage, new flow stress of the material is σ_2 and the surface strain is ε_2, which corresponds to σ_2. This work hardening process is continued until the ultimate strain is reached on the material surface. Steady state regime of mass loss is then achieved.

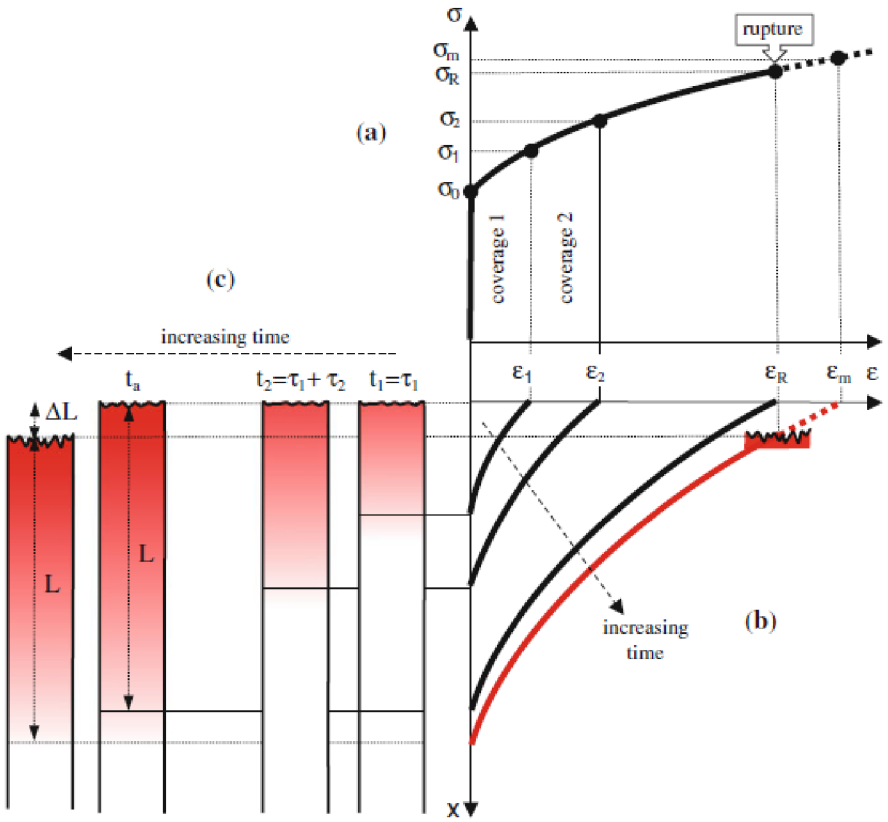

Figure 9 - Diagrams showing principle of erosion model a) stress-strain variation at the end of each coverage time, b) impact induced strain profile at the end of each coverage, c) change in geometry of specimen as a function of time, ta is duration of acceleration period [2]

3.2.1 Erosion rate during acceleration period

Flow stress progressively increases and work hardening develops during the acceleration period [24]. At the very beginning of exposure to cavitation, material is more ductile in general and dissipates a greater part of the impact energy by plastic deformation. As exposure time increases, eroded surface becomes work hardened and more brittle. This ductile damping effect decreases while the part of impact energy dissipated by elastic deformation and fracture becomes more important. Parallel to work hardening, surface roughness increases and cracks develop, which enhances the prospect of micro fractures and material loss. Already cracked and fractured zones are regions which are more likely to break away and to originate erosion because of stress concentration effects.

3.2.2 Erosion rate during steady state period

Impacts whose amplitudes exceed the material rupture strength, σ_U, are expected to damage the material during the steady state period. Key parameter in the model, in addition to the thickness of the hardened layer, L, is the coverage time, i.e. the time required for the material surface to be covered by erosive impacts. When a liquid drop hits the rigid surface, initial phase of impact involves compression of the liquid and generation of shockwaves. Liquid cramped between the shock front and solid surface near the contact zone is compressed, but the rest of the liquid drop is unsuspecting of impact. Both contact line and shock front spread over the impacted surface and at some point, the shock front separates from the contact edge because the velocity of the contact line decreases in time and falls below shock speed. Steady state period of erosion occurs as soon as the strain on the material surface reaches the rupture strain, ε_R, and from this time, strain profile inside the material does not change further and steady-state conditions are achieved [24].

After each new coverage, strain profile sinks into the eroded sample to a certain depth, which corresponds to thickness of the most superficial layer where the strain exceeds the value of rupture strain. Depth of this distortion is supposed to be removed by cavitation erosion according to failure criterion. This is the principle of computation of the erosion rate.

4 Analysis of available pitting tests and impact forces measurements

To use the phenomenological model for the prediction of cavitation aggressiveness, some experimental data is needed. Experiments need to be conducted in order to obtain erosion curves and data concerning diameters of pits which damage the material. These experiments are standardized and use standard equipment. Some of the most common ones are vibratory rigs, rotation discs, cavitation tunnels, cavitating jet cells and liquid jet devices [26]. Each of these tests give different erosion curves and different data can be obtained. What type of curve will be obtained depends greatly on the type of material and setup used during the test, e.g. distance from horn and the sample while using vibratory apparatus. Commonly tested materials are aluminum alloy, brass and stainless steel [26], [27], [28], [29]. Purpose of most experiments or laboratory tests for cavitation erosion is to predict material behavior under cavitation aggression. Different design features and operating parameters of equipment used for testing will result in different erosion rates. After the erosion tests are finished, eroded material can be observed using various devices. Micrographs and microscopes are the ones most commonly used [26], [27]. Further, data obtained with these devices can be used in e.g. MATLAB for in-depth processing and analysis.

When the material is exposed to cavitation, it becomes pitted and these pits can be measured with pitting tests. Material, theoretically, deforms only when the yield stress, σ_Y, is reached. With this said, a threshold for pitting tests is yield stress. This approach is valid in incubation period of cavitation, considering the fact that the pits are not overlapping during this period.

In pitting tests conducted by Aidoo [27], cumulative pitting rate for different exposure time interval was obtained. Aidoo conducted tests on aluminum alloy, which is the same material which was used in this study. Results demonstrate that the number of pits is increased when the exposure time is increased. As the pitting rate increases, there is a decrease in generation of larger pit volumes. Aidoo has obtained data about diameters as well. Values of these diameters were used in this

study, dependent on the time exposure to cavitation. Values of rate of impacts for various intervals obtained by Aidoo were also used in this study.

Cavitation impacts can be measured directly using Polyvinylidene Fluoride (PVDF) film. This is a sensor capable of converting mechanical energy into electrical energy. When cavitation is described, electrical signals are produced when the sensor is hit by a cavitation bubble. What is necessary to do when using PVDF film is a conversion of amplitude of the electrical signals into a corresponding force load. This leads to the analysis of the intensity of cavitation bubble collapse. Raw data obtained from PVDF film sensors is in the form of a graph with amplitude (voltage) on vertical, and time (seconds) on horizontal axis. Duran [5] has done experiments using PVDF film and her data has been used in this study.

Data necessary for phenomenological model explanation is obtained using aforementioned experiments. Most important values are closely connected to the device which is being used, properties of a material which will be used and the time necessary for an experiment to be conducted. Most significant data are obtained from experiments conducted by Aidoo and Duran, [27] and [5] respectively, and further Karimi and Leo [25], but other data should work with proposed phenomenological model, e.g. data from ICET database [26].

5 Model for the description of interaction between the cavitating flow and the impacted material

Previously described analytical model, see subsection 3.1, is presented to determine the cavitation erosion rate. As previously mentioned, the model considers properties of a material which is being eroded and the cavitation flow conditions. Mean level of stress amplitudes is controlled by the flow conditions and the erosion rate calculation unifies mechanical properties of a material being eroded, essentially rupture limit and the elastic limit, and material's metallurgical parameters, for instance work hardening exponent.

5.1 Core of the model

Goal of the model described by Karimi and Leo [25] is to describe the erosion rate as an explicit function of the material properties and of the hydrodynamic conditions of cavitation [25]. First step of the model is actually an erosion test under realistic cavitation conditions in order to obtain exact erosion curves. Throughout the early stage of erosion, erosion rate increases gradually as surface hardening occurs and expands over the entire exposed area. At this stage, accumulation of isolated damage leads to surface hardening, local fractures and crack propagation, all of which promote surface changes. Further on, the surface state remains roughly constant and damage then penetrates into the volume of the eroded material. Erosion rate at this stage remains constant and does not show fluctuations [29]. With this said, there are three main parameters to compute. Namely, erosion rate during the steady state period, $\dot{E}$, the exposure time after which erosion progresses at a constant rate, i.e. the border between the acceleration period and steady state, t_i, and the erosion rate during the acceleration period, $\dot{e}$ [25].

5.2 Erosion rate definition

The erosion rate can set certain limitations for design and it depends rigorously on cavitation aggressivity. Erosion rate, $\dot{e}$, is defined as instantaneous mass loss per unit time,

$$\dot{e} = \frac{dm}{dt} = \frac{d(\rho v)}{dt} = \rho \frac{dv}{dt} \qquad 3$$

where t is the time, m is the mass, v is the volume and ρ is the density of eroding material. Equation 3 can be written in a general form, as equation 4,

$$\dot{e} = \rho \frac{dv}{dt} = \rho \frac{dv}{dN} \frac{dN}{dt} \qquad 4$$

where N is the number of impacts generated by the collapse of cavitation bubbles.

5.3 Stress pulse amplitude distribution

Damaging power of erosive cavitation depends mainly on the intensity of the pressure pulses generated from the collapse of cavitation bubbles. To simplify, this parameter is represented by the height of the pressure peaks [25]. Distribution of these pulses is statistical and firstly probability density function of these pulse amplitudes was obtained experimentally [5]. Probability density function of stress pulses can be established using a curve-fitting method. Equation 5 gives the probability of obtaining a stress pulse amplitude σ originating from a cavity collapse for the given conditions.

$$P(\sigma) = A \cdot \sigma^{\alpha - 1} \cdot e^{\left(-\frac{\sigma}{\beta}\right)} \qquad 5$$

Parameters A, α and β are obtained from equation 5 using processing and analysis software, e.g. MATLAB. With the change of α and β, an extensive range of distribution shapes can be obtained.

5.4 Single damage size distribution

Erosion tests with an exposure time of only a few minutes were performed on the surface of the sample [27]. Purpose of the short-period tests was to exhibit enough impacts to be consistent statistically without overlap of impacts. Damages on the specimen, including indentations and pits of various sizes, can be made by impacts performed by collapses or from rebounds. Damaged areas are, after pitting test, observed and photographed by an optical microscope and using scanning electron microscopy (SEM) [27]. Using a quantitative image analyzer, area of the average diameter of each crater or hollow was measured.

Using the data gathered, a histogram of the number of impacts as a function of the measured damage size is made. Distribution was fitted using curve fit tool in MATLAB. This function of distribution is explained with equation 6 for material which was eroded and analyzed,

$$P(d) = \frac{1}{d \cdot \omega \cdot (2 \cdot \pi)^{\frac{1}{2}}} e^{\left\{-\frac{1}{2}\cdot\left(\frac{lnd-\mu}{\omega}\right)^2\right\}} \qquad 6$$

where μ and ω are obtained from the function of distribution.

5.5 Relation between real and measured damage size

Real deformation zone around the impacted area is larger than the zone measured by SEM observations [27]. Using SEM, only rough crater of the indentations is measured, but in reality, that indentation size is larger. To estimate the value of real indentation size, equation 7 is used,

$$\Delta\varepsilon_x = \Delta\varepsilon_0 \cdot \left(1 - \frac{x}{l}\right)^{\theta} \qquad 7$$

where the variables are: $\Delta\varepsilon_x$ is strain increment at a distance x from impacted point, $\Delta\varepsilon_0$ is strain increment induced at the impacted point, l is the depth of hardened layer and θ is a metallurgical parameter of the material denoting internal strain hardening. In Figure 10, calculated values are presented.

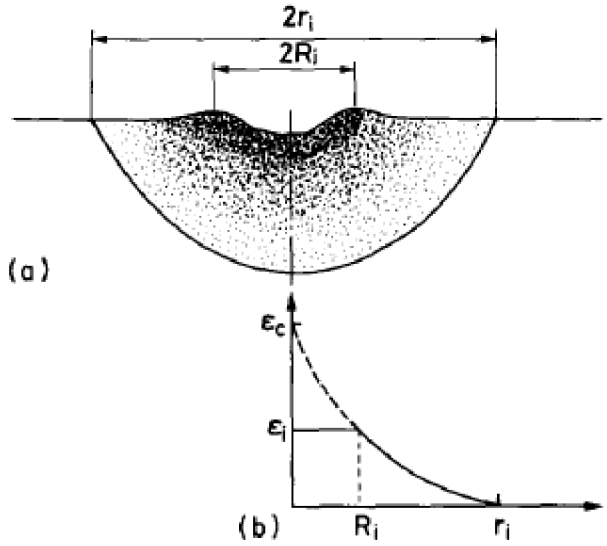

Figure 10 - (a) Relation between measured and real deformation zone diameter and (b) the profile of strain at impacted zone [25]

To estimate the real indentation radius r_i, we firstly use equation 8,

$$\varepsilon_i = \varepsilon_0 \cdot \left(1 - \frac{R_i}{r_i}\right)^{\theta} \qquad 8$$

which yields equation 9.

$$r_i = \frac{R_i}{1 - \left(\frac{\varepsilon_i}{\varepsilon_0}\right)^{\frac{1}{\theta}}} \qquad 9$$

Since $\varepsilon_i \ll \varepsilon_0$, we can obtain final equation in the form of equation 10,

$$r_i \cong R_i \cdot \theta \cdot \left(1 + \frac{\varepsilon_i}{\varepsilon_0}\right) \cong R_i \cdot \theta \qquad 10$$

where, in the end, R_i is the measured value of radii and θ is a metallurgical parameter explained previously.

5.6 Erosion rate during the steady state period

Current computational method describes the phenomenological principles of the erosion process. At the early stage of erosion, erosion rate is increased due to hardening of the exposed area and prolongation of damage over the entire eroded specimen. At the end of the stage where erosion rate is increased, situation comes to the state where the erosion rate is constant and this is named the steady state. In this model, the manifestation of erosion is attributed to the rupture strain, ε_R. When the impact-induced strain goes past the rupture limit, some part of the material is removed.

Using equation 8, and the relation between the stress and induced strain explained with equation 11, an equation 12 is obtained.

$$\sigma - \sigma_Y = K \cdot \varepsilon^n \qquad 11$$

$$(\sigma_U - \sigma_Y)^{\frac{1}{n}} = (\sigma_a - \sigma_Y)^{\frac{1}{n}} \cdot \left(1 - \frac{\Delta L}{L + \Delta L}\right)^{\theta} \qquad 12$$

From the equation 12, an expression for calculation of ΔL is made, presented in equation 13,

$$\Delta L = L \cdot \left\{ \left(\frac{\sigma_a - \sigma_Y}{\sigma_U - \sigma_Y} \right)^{\frac{1}{n \cdot \theta}} - 1 \right\} \quad 13$$

where σ_U is ultimate or rupture stress, σ_a is the impact stress pulse amplitude, σ_Y is material constant or material's yield strength, L is the maximum depth of hardened layer of eroded material, ΔL is the length of the rupture due to one cycle of impacts and n is the work hardening exponent.

Since the stress pulse amplitudes are distributed randomly, statistical average terms from equation 13 are used and modified equation 14 can be obtained,

$$\Delta L_m = L \cdot \left\{ \left(\frac{\sigma_{am} - \sigma_Y}{\sigma_U - \sigma_Y} \right)^{\frac{1}{n \cdot \theta}} - 1 \right\} \quad 14$$

where σ_{am} is the mean value of the stress pulse amplitudes beyond the ultimate stress of an eroded material. Value of σ_{am} is to be determined from probability density function of the stress pulses in equation 5. Equation 15 presents mean value of stress pulse amplitudes, σ_{am}, beyond ultimate stress of a certain eroded material.

$$\sigma_{am} = \frac{\int_{\sigma_U}^{\infty} A \cdot \sigma^{\alpha} \cdot e^{\left(-\frac{\sigma}{\beta}\right)} d\sigma}{\int_{\sigma_U}^{\infty} A \cdot \sigma^{\alpha-1} \cdot e^{\left(-\frac{\sigma}{\beta}\right)} d\sigma} \quad 15$$

Total impact number, N, for an exposure time t is presented in equation 16.

$$N = \dot{N} \cdot t \quad 16$$

In equation 16, $\dot{N}$ is the rate of impacts. Total number of impacts, which contribute to breaking of the material and material loss in the end, becomes N_p, explained with equation 17.

$$N_p = \dot{N} \cdot t \cdot \{1 - P(\sigma_U)\} \quad 17$$

In equation 17, $P(\sigma_U)$ is defined with equation 18.

$$P(\sigma_U) = \int_0^{\sigma_U} A \cdot \sigma^{\alpha-1} \cdot e^{\left(-\frac{\sigma}{\beta}\right)} d\sigma \quad 18$$

Some of the impacts are distributed over the material's surface and they do not propagate damage into the material's volume. They are explained with equation 19,

$$N_s = \frac{S_0}{S_m} \tag{19}$$

where S_0 is an exposed area and S_m is the average size of impacts. Average size of impacts, S_m, is defined with equation 20,

$$S_m = \frac{{d_m}^2 \cdot \pi}{4} \tag{20}$$

where d_m is the average damage size determined from equation 6. Furthermore, there are impacts which propagate damage into the volume, expressed with equation 21.

$$N_h = \frac{N_P}{N_s} \tag{21}$$

Total eroded depth after certain exposure time t is obtained from equation 22.

$$h(t) = \frac{\dot{N} \cdot t \cdot \{1 - P(\sigma_U)\}}{\frac{S_0}{S_m}} \cdot \Delta L_m \tag{22}$$

Erosion rate is then obtained using the equation 25.

$$\dot{E} = \frac{dm}{dt} = \rho \cdot \frac{dv}{dt} = \rho \cdot \frac{d}{dt} \cdot \{S_0 \cdot h(t)\} = \rho \cdot \ S_0 \cdot \frac{d}{dt} \cdot h(t) \tag{23}$$

$$\dot{E} = \rho \cdot \dot{N} \cdot t \cdot \{1 - P(\sigma_R)\} \cdot S_m \cdot \Delta L_m \tag{24}$$

$$\dot{E} = \rho \cdot \ S_m \cdot \dot{N} \cdot L \cdot \left\{ \left(\frac{\sigma_{am} - \sigma_Y}{\sigma_U - \sigma_Y} \right)^{\frac{1}{n \cdot 0}} - 1 \right\} \cdot \left\{ 1 - \int_0^{\sigma_U} A \cdot \sigma^{\alpha - 1} \cdot e^{\left(-\frac{\sigma}{\beta} \right)} d\sigma \right\} \tag{25}$$

6 Cavitation erosion tests for the validation of the aggressiveness model

Cavitation erosion tests are conducted in order to evaluate the resistance of different materials to erosion. This erosion depends on both the properties of eroded material and on the way that cavitation is generated. There are four main groups of cavitation erosion laboratory testing, and they are divided based on the way the cavitation is generated. Four main groups are:

- ASTM G-32 vibratory apparatus,
- cavitating liquid jets ASTM G-134,
- cavitation tunnels
- rotating disc apparatus [30].

Vibratory test method using vibratory apparatus ASTM G-32 with stationary specimen is further explained since it was used for the experimental part of this study.

6.1 Cavitation erosion testing using ASTM G-32 vibratory apparatus

Cavitation erosion develops on material surfaces which are exposed to intense ultrasonic cavitation. Cavitation erosion testing is a fast method to measure erosion resistance of materials or coatings to intense stress and other erosion factors.

6.1.1 Description of experimental setup

A vibratory cavitation test device ASTM G-32 was utilized in this study. It is an ultrasonic device UIP1000hdT made by Hielscher Ultrasonics comprised of an ultrasonic transducer which is attached to an ultrasonic horn. This ultrasonic horn is vibrating at certain frequency of $20 \pm 0.2\ kHz$ with amplitude of 57 μm which can be adjusted from $50\ to\ 100$ % [5], [31]. Cavitation erosion test properties are presented in Table 1.

Table 1 - Cavitation erosion test properties

Name of parameter	Value	Unit
Frequency of vibration	20 ± 0.2	kHz
Vibration amplitude	57	μm
Gap between sample and horn	0.5	mm
Temperature of water	20 ± 1	°C

Vibratory apparatus couples ultrasonic vibrations into liquids, such as water, and fast movement of the vibration in the liquid is responsible for production and collapse of cavitation bubbles. Real experimental setup from the laboratory is given in Figure 11 and sketch of same experimental setup with components is presented in Figure 12.

In order to test sample using a vibratory apparatus it is necessary to clean the sample thoroughly [27]. Prior to mounting the sample in the holder, it is weighed. Weighing is done in order to track mass loss, using a precision scale with accuracy of 0.001 g. Sample is placed in a holder and secured using three tighteners. Rubber band is secured in the apparatus in order to prevent any leaks. Holder is then placed with the sample under an ultrasonic horn at a distance of around 0.5 mm. This distance is very important since it affects the speed of the test itself and results afterward. After specimen is set in correct place, everything must be tightened with fasteners from below otherwise water would run out and the test itself would not work properly. Fluid which is commonly used for this kind of apparatus is distilled water. Water is poured into the cavitation erosion tester fully and carefully, and temperature sensor is inserted into a designated checking tube. Laboratory tap water supply was used in order to keep the temperature of the working fluid at around 20°C. After all the equipment was connected and secured in place, test could start. Cooler was also a part of this experiment in order to cool down the transducer from the outside. Generator is connected to transducer and powering it on, experiment starts. As soon as the experiment starts, piercing sound surrounds the laboratory and thus the reason for use of hearing equipment. Once vibrations start to occur, fluid starts to affect specimen rapidly, and this causes damage to its surface. This experiment was interrupted in intervals of 30 and later 60 minutes in order to

gather data about specimen weight, which can then be tracked over chosen period of time. Since the distance from the ultrasonic horn to the specimen was short, i.e. 0.5 *mm*, the acceleration period of cavitation started very soon. If the distance were to be longer, e.g. 2.5 *mm* or 5 *mm*, it would take more time to reach acceleration period. More about the results of the experiment and when the mass loss started to occur and then became constant is presented in article 7.1.1 of this study.

Figure 11 - Experimental setup

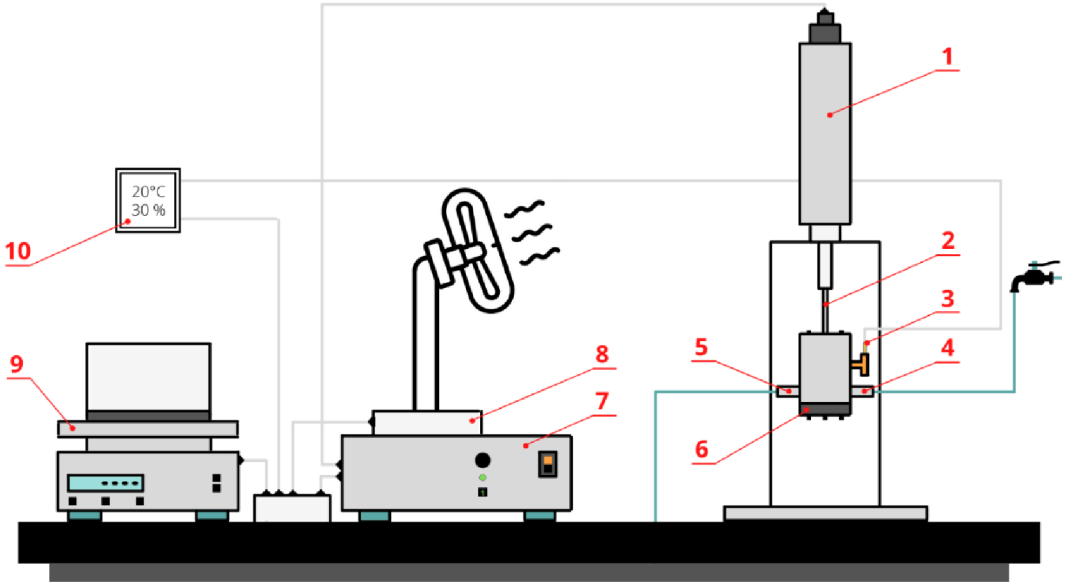

Figure 12 - Sketch of experimental setup with components, where: 1-transducer, 2-ultrasonic horn, 3-temperature sensor, 4-water inlet, 5-water outlet, 6-holder with sample in place, 7-generator, 8-cooler, 9-digital scale and 10-thermometer

6.2 Description of sample material

Experiment was conducted on aluminum alloy EN AW-7075 T6511 [27]. Chemical composition of this material is presented in Table 2. This is a material used especially where a combination of high hardness and low weight is important, e.g. automotive industry, machine building and similar. Since this aluminum is alloyed with copper, this alloy has a decreased corrosion resistance in atmospheric conditions [32].

Table 2 - Chemical composition of test sample [27]

Chemical composition							
%							
Zn	Mg	Cu	Cr	Fe	Mn	Si	Ti
6.00	2.60	1.50	0.20	0.19 *to* 0.20	0.16	0.10	0.04

Mechanical properties of this material are presented in Table 3.

Table 3 - Mechanical properties of the test sample [27]

Mechanical properties			
Name	Notation	Value	Unit
Tensile strength	σ_U	576	MPa
Yield strength	σ_Y	521	MPa
Elongation	ε	8.5	%

6.3 Description of sample preparation

Different methods were used in sample preparation, including dimensioning and surface polishing techniques. Sample was machined according to the dimensions presented in Figure 13. Surface of the test sample was firstly subjected to grinding on sandpaper. To move closer to the smooth finish of the sample, two sandpaper grits were used. Namely, 600-grit and 1200-grit sandpaper. Higher grits deliver a smoother finish. Sample was washed with water and sprayed with cleaning alcohol

before drying using a hand dryer. To obtain mirror-like finish, polishing cloths were used [27].

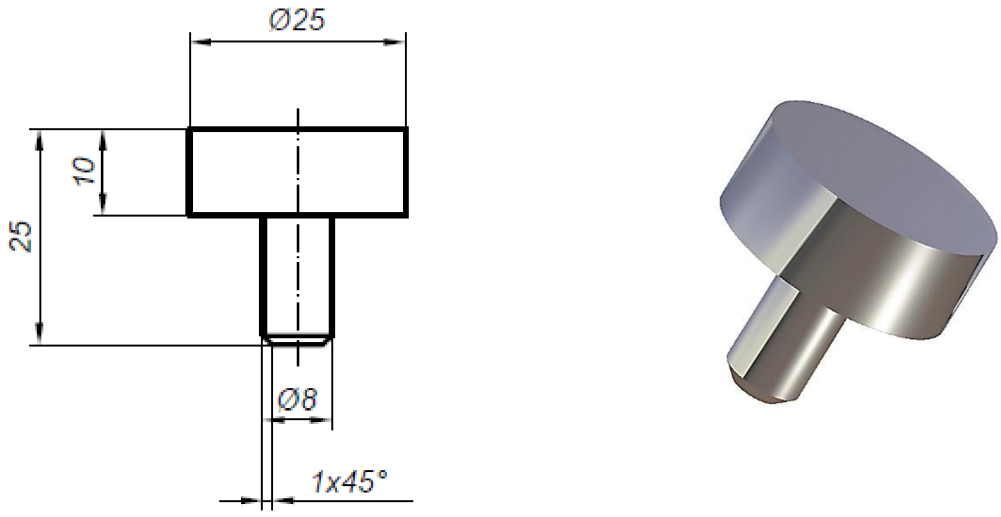

a) *b)*

Figure 13 – Sample, a) sketch with dimensions, b) 3D model

6.4 Holder preparation and description

Holder was also produced for this experiment since the sample dimensions are not standard for use on this specific apparatus. For experiment itself, holder is placed under a horn with sample in place and distance is set according to experiment needs. For this experiment, distance was set to 0.5 *mm*. Holder is then, with sample, secured with tighteners in order to keep the cooling and cavitating fluid inside. If the tightening would not be done properly, all water would leak out and experiment would fail. In Figure 14, most important dimensions of holder are presented, which are dimensions in direct relation to the sample. In Figure 15, top and bottom view of the holder is visible. Figure 16 presents 3D model of a holder with sample in place, prepared for testing on ASTM G-32 vibratory apparatus.

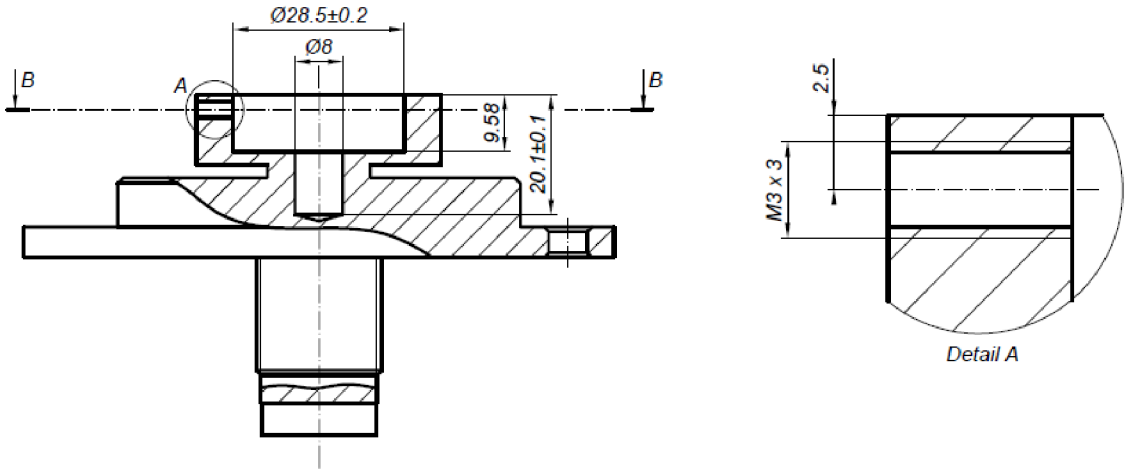

Figure 14 - Side view of holder with detail A

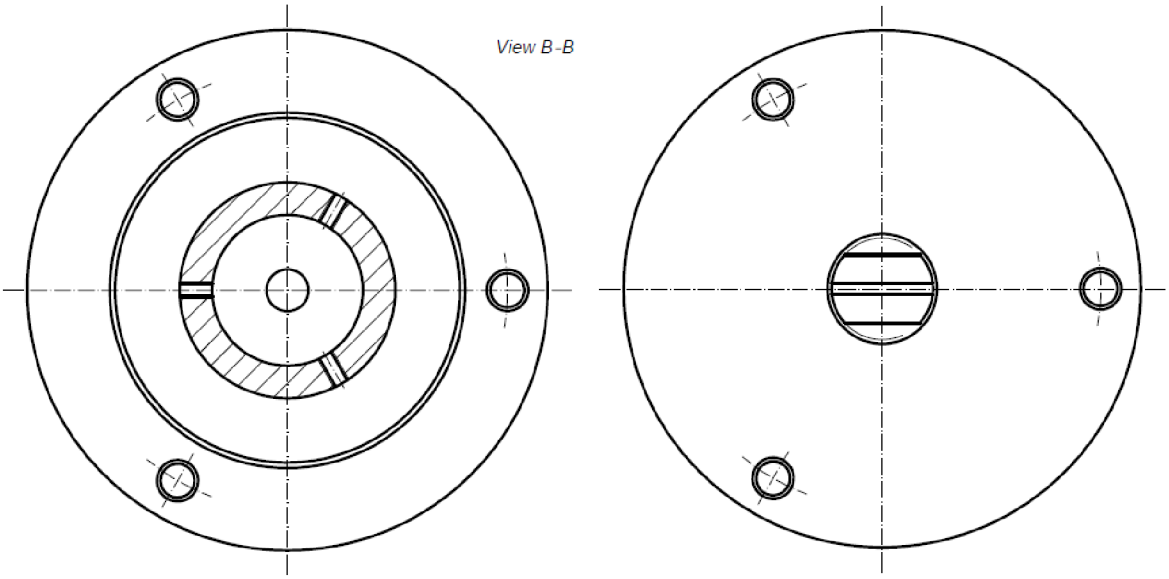

a) *b)*

Figure 15 - Top view of a holder (a), with view B-B;
bottom view (b) of a holder

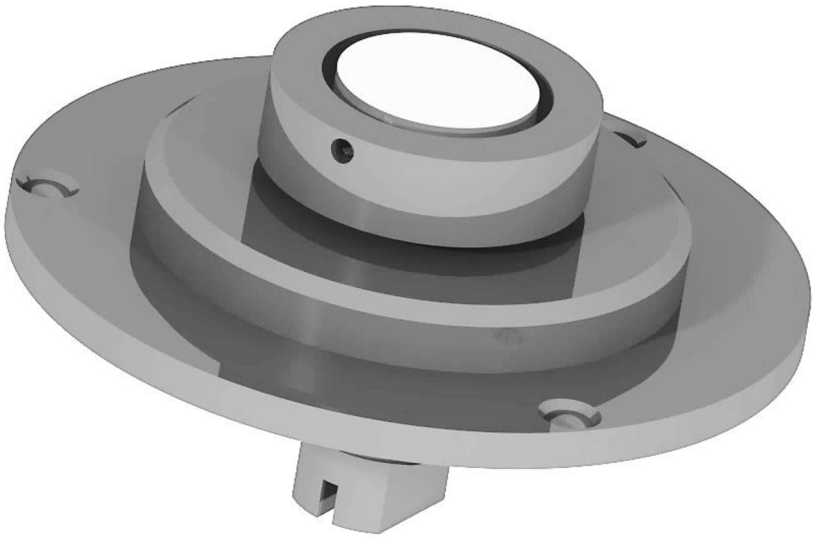

Figure 16 - 3D model of the holder with sample in place

7 Application of the phenomenological model for the prediction of cavitation aggressiveness

During analytical work of this study it was found that some coefficients related to experimental data connected to cavitation are needed. That experimental data is obtained within this study and analytical work is further concluded.

7.1 Results and discussion

Results are divided into two parts: one part is connected to experiment conducted on vibratory apparatus and other part is connected to the analytical approach using a phenomenological model for prediction of cavitation erosion rate.

7.1.1 Results obtained experimentally

Detailed description of apparatus and its components is found within article 6.1.1 and material used for the experiment on this apparatus is explained in subsection 6.2 of this study.

When using this apparatus for cavitation erosion measurement, mass loss curve can be obtained. Mass loss data is necessary for phenomenological model for prediction of cavitation erosion rate, specifically, for further comparison of obtained results. Incubation and acceleration period during cavitation were not of interest for this study. Steady state period is, and that is why experiment was conducted until steady state was reached and mass loss became of approximately constant value. Weight measurement was done using digital scale. Sample was weighed before the experiment and then after set intervals. Firstly, intervals were set to 30 minutes and later they were increased to 60 minutes. Mass loss curve was obtained with gathered data and is presented in Figure 17.

Experiment was conducted during two-day period. In this time, incubation period was passed during first day and during second day acceleration period as well. Steady state period was reached during second day. The test took 510 minutes to reach constant steady state, see red dashed line in Figure 17. Test was interrupted after this time and data visible in Figure 17 is approximated for time after

510 minutes. Dashed blue curve represents approximation of values for erosion rate. Assumption is that the steady state continues over a long period of time.

It is noticeable that the incubation period for this material and for this experimental setup is very short. This is due to material characteristics and its chemical composition. This experimental curve presented in Figure 17 can be compared to theoretical curve presented in Figure 6. When comparing the two curves, experimentally obtained curve follows the same trend as a theoretical one.

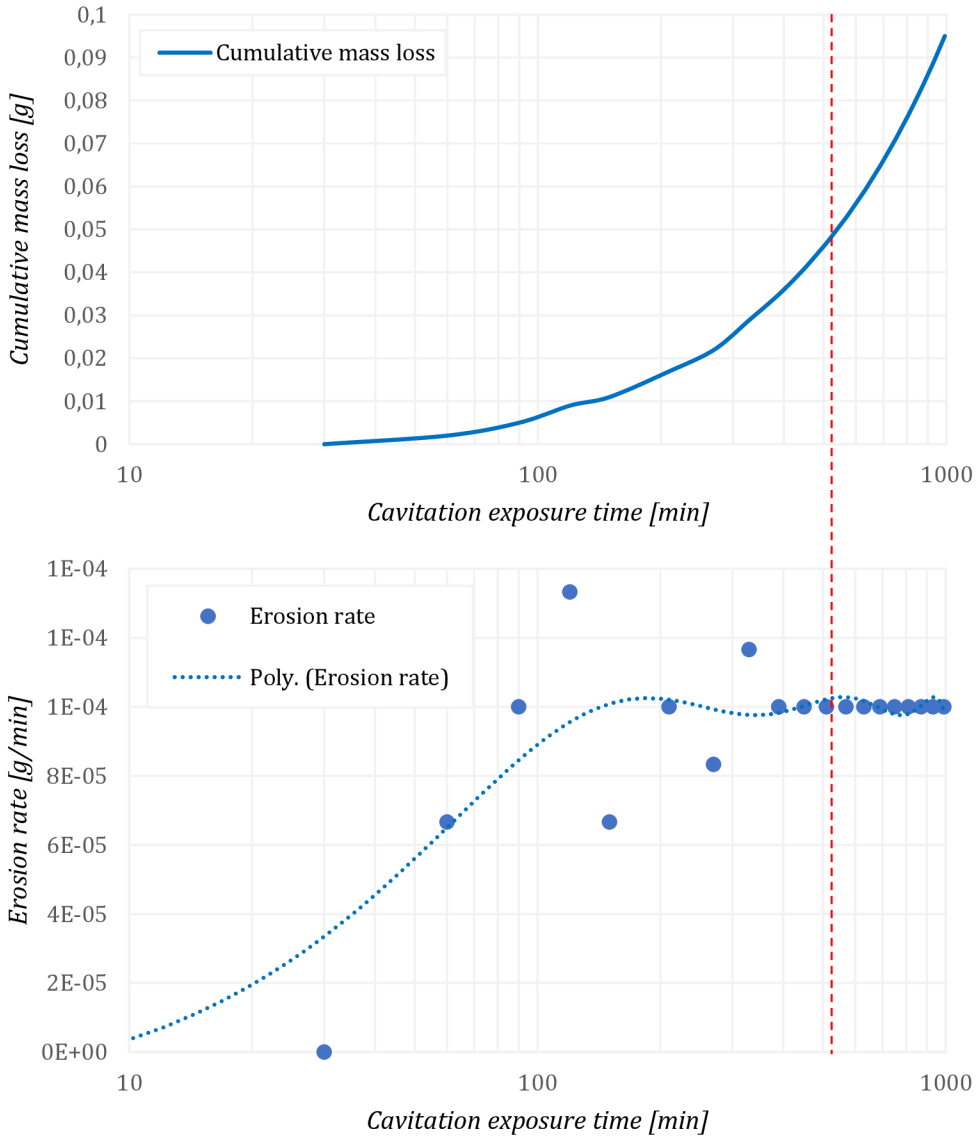

Figure 17 – Experimentally obtained curve for cumulative mass loss (top graph) and curve for erosion rate (bottom graph) over time

7.1.2 Results obtained analytically

To test the validity of the model presented in section 5, model was applied to aluminum alloy EN AW-7075 T6511 for which experimental curve was obtained and presented in article 7.1.1 of this study. Other models for prediction of cavitation erosion aggressiveness work in similar way. Acceleration period is the most complicated part of cavitation erosion since almost every significant change on the material's surface and every observable phenomenon occurs during this period. Steady state period occurs after the acceleration period ends and continues for a long period of time and during this time, as observed in Figure 17 and theoretical curve, Figure 6, mass loss becomes approximately constant. Constants needed for the analytical solution are obtained with available experimental data, visible in section 4.

Stress pulse amplitude distribution

To obtain stress pulse amplitude distribution, a piezo stress constant is needed for PVDF film, as well as thickness of PVDF film. These values are presented in Table 4.

Table 4 - PVDF film parameters [33]

Name	Notation	Value	Unit
Piezo stress constant	g_{33}	330	$\frac{V}{m} \Big/ \frac{N}{m^2}$
Thickness of PVDF film	t_{PVDF}	28	μm

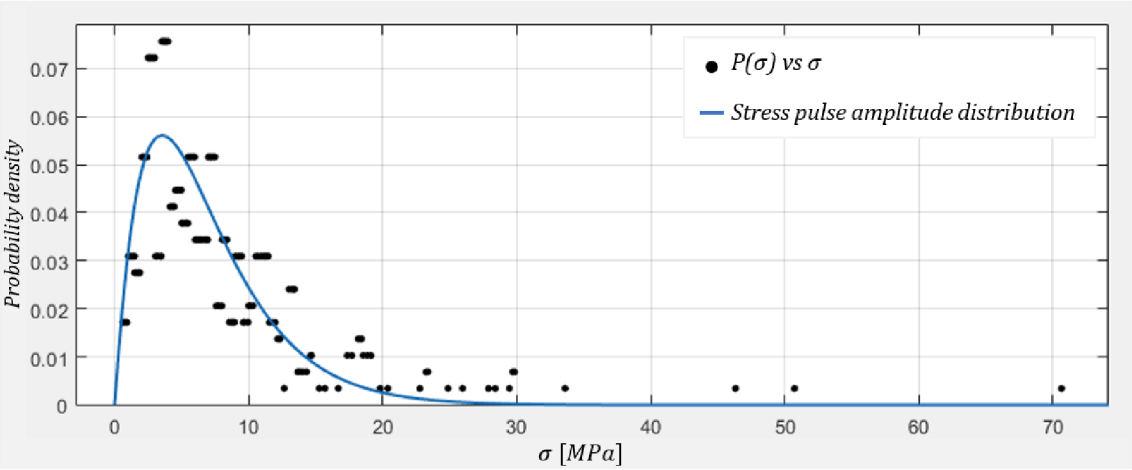

Figure 18 – Curve-fitted shape of the number of impacts as a function of amplitude of the pulses in cavitation collapse

Values presented in Table 4 are recalculated with known voltage values obtained by Duran [5]. Stress pulse amplitude distribution is presented in Figure 18.

MATLAB was used to solve the function of stress pulse amplitude distribution, i.e. equation 5, presented in subsection 5.3, as well as function of distribution, i.e. equation 6, presented in subsection 5.4. Solving these functions, parameters A, α, β, ω and μ are obtained. Values of these parameters are presented in Table 5. All the parameters are dimensionless numbers.

Table 5 – Parameters obtained in MATLAB

Name	Notation	Value for ASTM G-32 vibratory rig
Parameter in $P(\sigma)$	A	0.04229
Shape parameter in $P(\sigma)$	α	2.059
Scale parameter in $P(\sigma)$	β	3.347
Shape parameter in $P(d)$	ω	2.699
Parameter in $P(d)$	μ	0.5487

Single damage size distribution

Single damage size distribution curve is presented in Figure 19, which is a solution for the equation 6. Curve shows the probability density in relation to the pit diameters for the interval of 80 s [27].

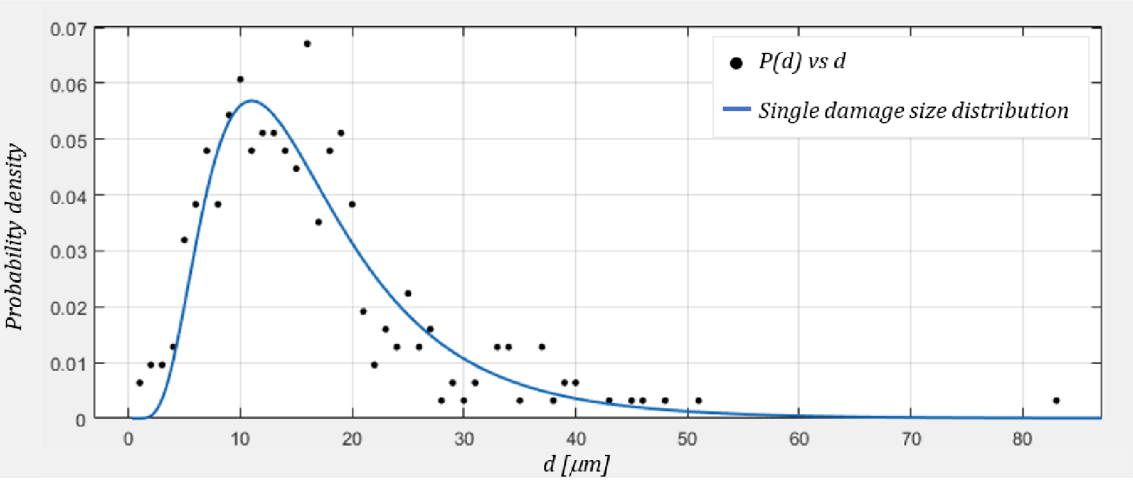

Figure 19 – Curve-fitted shape of the number of impacts as a function of their size

Relation between real and measured damage size

To make a relation between real and measured damage size, equation 10 is used, presented in subsection 5.5. In this equation, radii of observable pits which is the actual damage on the material is needed. Diameters of the pits for several time intervals are obtained in study done by Aidoo *[27]*. If one specific time period is observable, a comparison between real and measured damage size can be made. One material property which is needed to solve equation 10 is internal strain hardening parameter, θ, whose value is presented in Table 6.

With this known parameter, comparison is done and presented in Figure 20. It is noticeable that value of real size greatly depends on the material, i.e. metallurgical parameter of the material, in a way that the difference between the real and measured damage size will be greater if the parameter has bigger value.

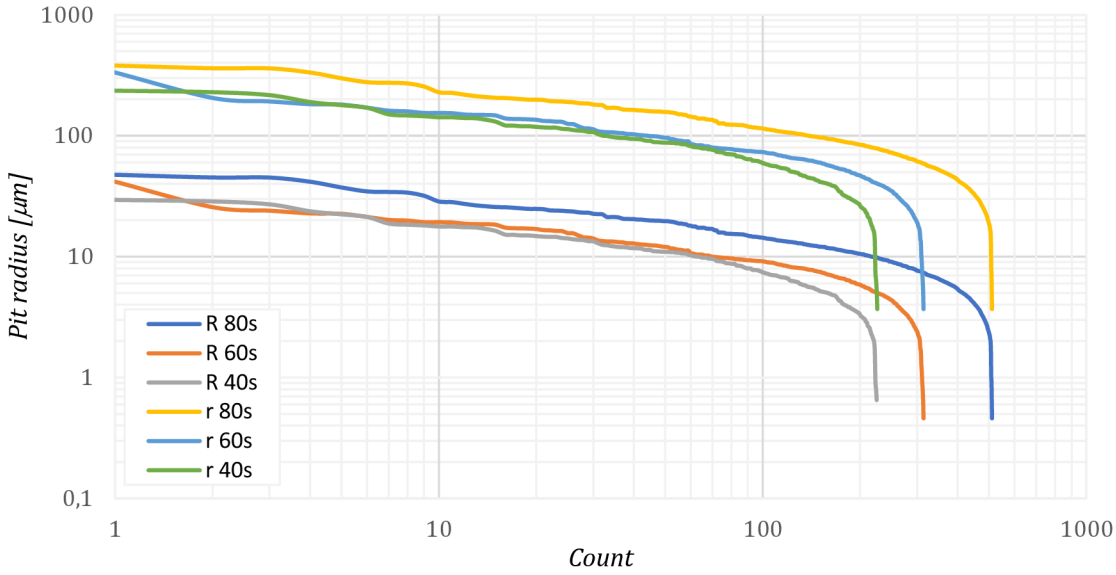

Figure 20 - Graphical representation of relation between real and measured damage size

For Figure 20, r is the real radius of a pit, and R is the measured radius of a pit, see subsection 5.5.

Erosion rate during steady state period

For determination of erosion rate during steady state period, equation 25 is used. However, it depends on multiple values, such as stress pulse amplitude of impact, rate of impacts, various material properties and previously computed parameters A, α and β. Using equation 15, mean value of the stress pulse amplitudes beyond the ultimate stress of an eroded material, σ_{am}, is estimated.

Value of σ_{am} is obtained using MATLAB by *integral* function and equation 15, and the value is obtained to be $\sigma_{am} = 579.37\ MPa$. Since obtained value is higher than the ultimate stress value of this material, see Table 6, it is acceptable for this study.

Table 6 – Properties of aluminum alloy

Material property	Notation	Value	Unit
Ultimate (tensile) strength	σ_U	576	MPa
Yield strength	σ_Y	521	MPa
Elongation	ε	8.5	%
Density	ρ	2810	$^{kg}/_{m^3}$
Hardening exponent	n	0.17	-
Internal strain hardening parameter	θ	8	-

Further, length of rupture due to one cycle of impacts, ΔL_m, can be obtained using equation 14. Value of ΔL_m is also obtained in MATLAB and it is $\Delta L_m = 4.47\ \mu m$. Maximum depth of hardened layer for material used in this study is estimated to be $L = 100\ \mu m$ and other values of material properties necessary for determination of ΔL_m are presented in Table 6.

Using equation 16, rate of impacts can be obtained with known time of exposure and total number of impacts on the observed area. Observed area is found in study of Aidoo [27], and it is $S_0 = 4\ mm^2$. Rate of impacts is e.g. $\dot{N} = 2100.43\ ^{count}/_{s}$ or recalculated to minutes, $\dot{N} = 126025.5\ ^{count}/_{min}$. This is valid for $80\ s$ time interval. Other obtained values of rate of impacts for various time intervals are presented in Table 7.

Table 7 - Rate of impacts

Time interval, t	Rate of impacts, $\dot{N}$	Total number of impacts, N
40 s	$727.78\ ^{count}/_{s}$	29111
60 s	$1052.17\ ^{count}/_{s}$	63130
80 s	$2100.43\ ^{count}/_{s}$	168034

For determining the total number of impacts which contribute to rupture and material loss, equation 17 is used. In this equation, unknown parameter, $P(\sigma_U)$, is obtained using MATLAB and equation 18. It has a value $P(\sigma_U) = 0.52$. With this

value known, N_p can be obtained for various time intervals, which is presented in Table 8. Values were rounded to the nearest integer.

Table 8 – Total number of impacts which contribute to material loss

Time interval, t	Total number of impacts which contribute to material loss, N_p
40 s	13909
60 s	30164
80 s	80287

Mean value of diameters, necessary to solve equations 19 and 20 is obtained using single damage size distribution, i.e. equation 6. Values of diameters are taken from study by Campo [5]. Since time interval is different and different pit sizes occur in each time interval, values are presented in Table 9. Average size of the impacts, S_m, is estimated using equation 20 and presented in Table 9 as well.

Table 9 - Mean values of diameters and average size of the impacts

Time interval, t	Mean value of diameters, d_m	Average size of impacts, S_m
40 s	15.96 μm	200.03 μm^2
60 s	16 μm	201.14 μm^2
80 s	20.74 μm	337.7 μm^2

From equation 19, impacts distributed over material's surface which do not propagate damage into the material's volume, N_s, are obtained. They are presented in Table 10 and they are rounded to the nearest integer. Values of N_h, ratio of total number of impacts which contribute to material loss and number of impacts which do not propagate into the volume are presented in as well, and obtained with equation 21.

Table 10 – Number of impacts N_s and ratio N_h

Time interval, t	Impacts which do not propagate into the volume, N_s	Ratio of impacts, N_h
40 s	19997	0.67
60 s	19887	1.52
80 s	11845	6.78

Total eroded depth after some exposure time is estimated using equation 22. It depends on time of exposure, and it is presented in Table 11.

Table 11 – Values of total eroded depth, $h(t)$

Time interval, t	Total eroded depth, $h(t)$
40 s	3.11 μm
60 s	6.77 μm
80 s	30.27 μm

Ultimately, erosion rate is obtained using equation 25. Values of erosion rate, $\dot{E}$, are presented in Table 12 and it is visible that erosion rate is constant for steady state period of cavitation.

Table 12 – Values of erosion rate, $\dot{E}$

Time interval, t	Erosion rate, $\dot{E}$		
40 s	$8.73 \cdot 10^{-10}\ {}^{kg}/_{s}$	$5.24 \cdot 10^{-8}\ {}^{kg}/_{min}$	$3.14 \cdot 10^{-6}\ {}^{kg}/_{h}$
60 s	$1.27 \cdot 10^{-9}\ {}^{kg}/_{s}$	$7.62 \cdot 10^{-8}\ {}^{kg}/_{min}$	$4.57 \cdot 10^{-6}\ {}^{kg}/_{h}$
80 s	$4.25 \cdot 10^{-9}\ {}^{kg}/_{s}$	$2.55 \cdot 10^{-8}\ {}^{kg}/_{min}$	$1.53 \cdot 10^{-5}\ {}^{kg}/_{h}$

7.1.3 Discussion regarding analysis of the model applicability for the cavitation aggressiveness prediction

Analysis of model applicability is directly connected to the experimental erosion test, see article 7.1.1. After completion of this test, explained in detail in article 6.1.1 of this study, an erosion curve is obtained and steady state mass loss is reached after certain amount of erosion cavitation time, see Figure 17. Value of erosion rate obtained with erosion experiment on vibratory cavitation test device corresponds to $\dot{E} = 1 \cdot 10^{-4} \left[{}^{g}/_{min}\right] = 6 \cdot 10^{-6} \left[{}^{kg}/_{h}\right]$. This value is compared to the value obtained with the phenomenological model for cavitation erosion prediction and it is visible in Table 13.

Table 13 - Comparison of obtained data

Method	$\dot{E}$ value	Unit
Analytical	$3.14 \cdot 10^{-6}$	${}^{kg}/_{h}$
	$4.57 \cdot 10^{-6}$	${}^{kg}/_{h}$
	$1.53 \cdot 10^{-5}$	${}^{kg}/_{h}$
Experimental	$6 \cdot 10^{-6}$	${}^{kg}/_{h}$

Data obtained analytically is comparable to the experimentally obtained data. It is clear that the values are of the same order and it is sufficient to say that the model is applicable for the erosion test done in this study, with use of experimental data obtained in the studies of Aidoo [27] and Duran [5]. In order to use the experimental data, it must be obtained from the same cavitation erosion testing device under same conditions and on the same sample material. This is approximated for the cases of aforementioned studies since the sample used in this study has been manufactured and prepared during the experimental work of Aidoo. Experimental setup is almost similar, excluding the gap between the sample and horn. It is clear that the data obtained with utilization of relatively quick experiment can be used in the phenomenological model presented in this study.

As visible in Figure 17, there is a clear distinction between acceleration and steady state period of cavitation on both graphs. Blue points on the bottom graph represent the data gathered during the experiment and dashed blue line represents approximation of that data using polynomial fit. Polynomial fit was done using Excel for the whole time period. If the polynomial fit could have been done only for the acceleration period using a polynomial or some other curve fitting method, e.g. Gaussian, blue dashed line would follow a trend very similar to the trend presented in Figure 6. However, it is known that there is no mass loss during the incubation period of cavitation erosion and that is clear from the top graph of Figure 17, where cumulative mass loss is presented, so the graphs are both valid if used together. Regarding the cumulative mass loss, it follows the same trend as presented in the model by Karimi and Leo [25] in a way that it becomes linear after steady state has been reached. To improve the curves of erosion rate and cumulative mass loss, an improvement in experiment itself needs to be made, see section 8 of this study. Experimental data obtained by Aidoo [27] and Duran [5] is usable and the accuracy of conducted experiments is never 100% correct since there are multiple factors which can, in the end, affect the final result. Experiments need to be done multiple times with multiple breaks to check repeatability and certainty of results.

8 Conclusion

Goal of this study was to prove that analytical phenomenological model presented by Karimi and Leo [25] is applicable to certain material and certain experimental setup. Phenomenological model was proven to be valid for steady state period of cavitation, for aluminum alloy with smooth surface finish and experimental data obtained on vibratory apparatus.

In order to clarify the model, research on models which are used for description of cavitation aggressiveness and erosion is concluded. Further, material response to the cavitating flow impact and the analysis of available measurements from pitting tests and impact forces is studied. Experiment is conducted in order to acquire mass loss data which is compared to analytically obtained results. Experimental data obtained in this study is compared to the pitting data evaluated in study of Aidoo [27]. Data differs in such a way that, initially, the experimental setup is set in a different way, i.e. sample in this study is set at a distance of 0.5 mm from the horn, whereas in the study of Aidoo it was set to 2.5 mm. With this said, some deviations in results are expected. Moreover, in the study of Duran [5], PVDF film was used for measurement. In this study, data obtained by Duran, i.e. impact forces, is recalculated in a connection with piezo constant, which is not always the correct approach since piezo constant depends on many parameters and in this study general value was used, see Table 4. Normally, for measurement of pressure, some pressure sensor is to be utilized in order to avoid recalculations. Data does not differ in the sample material since the material is the same for both studies. However, the sample was manufactured and polished for study of Aidoo [27], and since some time has elapsed from then, it is expected that the sample has lost the fine polished surface qualities. Nevertheless, it is the same sample and data can be compared. Possible improvement regarding the pitting test is to measure more points and to interrupt the measurement multiple times to gather more data between. Regarding the impact forces measurement, pressure sensor can be utilized instead of piezo constant and data transformation using this constant.

Main idea is that there are relatively simple experiments which can be conducted in a very short period of time. With experimental data in gathered and processed, it is further usable in the phenomenological model as is the one presented by Karimi and Leo [25]. Model needs to be correlated to erosion rate and cumulative mass loss curves, see Figure 6 and Figure 17 obtained experimentally. Analytical model utilizes mechanical and metallurgical parameters of materials and that is the advantage of this model. Model is yet to be utilized in the acceleration period of erosion, which is more complicated and not a part of this study, mainly because of time limitations.

In conclusion, experiments conducted in couple of minutes are able to predict cavitation erosion over hundreds of hours or in other words, there exists a possibility to predict cavitation erosion based on simple experimental measurements done.

REFERENCES

[1] C. E. Brennen, "An Introduction to Cavitation Fundamentals," in *Cavitation: Turbo-machinery & Medical Applications*, Warwick, UK, 2011.

[2] J.-P. Franc, K.-H. Kim, A. Karimi and G. Chahine, Advanced Experimental and Numerical Techniques for Cavitation Erosion Prediction, Springer, 2014.

[3] H. Kotoulová, "Cavitation erosion mechanisms (Bachelor thesis)," Brno University of Technology, Brno, Czech Republic, 2019.

[4] J. G. Garcia, V. Sáez, I. Tudela, M. I. D. Garcia, M. D. Esclapez and O. Louisnard, "Sonochemical Treatment of Water Polluted by Chlorinated Organocompunds, A Review," *Water,* no. 2, pp. 28-74, 2010.

[5] M. M. C. Duran, "Investigation of the Cavitation Aggressiveness Using PVDF Sensors (Master thesis)," Technical University of Liberec, Liberec, Czech Republic, 2019.

[6] D. L. Miller, S. V. Pislaru and J. F. Greenleaf, "Sonoporation: Mechanical DNA Delivery by Ultrasonic Cavitation," *Somatic Cell and Molecular Genetics,* pp. 115-134, 2002.

[7] C. E. Brennen, Cavitation and Bubble Dynamics, New York, USA: Cambridge University Press, 2014.

[8] C. E. Brennen, Fundamentals of Multiphase Flows, Pasadena, California, USA: Cambridge University Press, 2005.

[9] T. B. Benjamin and A. T. Ellis, "The Collapse of Cavitation Bubbles and the Pressures thereby Produced against Solid Boundaries," in *Philosophical Transactions of the Royal Society of London. Series A, Mathematical and Physical Sciences*, London, UK, The Royal Society Publishing, 1966, pp. 221-240.

[10] S. C. Roy, "Modeling and analysis of material behavior during cavitation erosion (Doctoral dissertation)," Université Grenoble Alpes, Grenoble, France, 2015.

[11] O. Supponen, "Collapse phenomena of deformed cavitation bubbles (Thesis)," Swiss Federal Institute of Technology Lausanne (École Polytechnique Fédérale de Lausanne), Lausanne, Switzerland, 2017.

[12] J.-P. Franc and J.-M. Michel, Fundamentals of Cavitation, Kluwer Academic Publishers, 2005.

[13] R. P. Tong, W. P. Schiffers, S. J. Shaw, J. R. Blake and D. C. Emmony, "The role of "splashing" in the collapse of a laser-generated cavity near a rigid boundary," *Journal of Fluid Mechanics,* vol. 380, pp. 339-361, 1999.

[14] "UNSW, School of Materials Science and Engineering: Yield Strength," [Online]. Available: https://www.materials.unsw.edu.au/study-us/high-school-students-and-teachers/online-tutorials/stress-and-strain/stress-and-strain/yield-strength. [Accessed May 2021].

[15] J.-P. Franc, "Incubation time and cavitation erosion rate of work-hardening materials," *Journal of Fluids Engineering,* 2009.

[16] "Flow Stress," [Online]. Available: https://www.princeton.edu/~maelabs/mae324/glos324/flowstress.htm. [Accessed January 2021].

[17] "iMechanica," [Online]. Available: https://imechanica.org/node/4692. [Accessed January 2021].

[18] "Proto: Residual stress info," [Online]. Available: https://www.protoxrd.com/knowledge-center/residual-stress-info. [Accessed January 2021].

[19] R. A. Sai, "The improvement of the cavitation resistance of technical surfaces using high power laser pulses," Technical University of Liberec, Liberec, Czech Republic, 2020.

[20] P. P. Shukla, P. T. Swanson and C. J. Page, "Laser shock peening and mechanical shot peening processes applicable for the surface treatment of technical grade ceramics: A review," *Journal of Engineering Manufacture,* p. 639–652, 2013.

[21] T. Suhonen, J. Laakso, M. Jokipii, P. Vuoristo and T. Varis, "Evaluation of Residual Stresses and Their Influence on Cavitation Erosion Resistance of High Kinetic HVOF and HVAF-Sprayed WC-CoCr Coatings," *Journal of Thermal Spray Technology,* vol. 29, pp. 1365-1381, 2020.

[22] G. Chahine, "Modeling of Cavitation Dynamics and Ineraction with Material," in *Advanced Experimental and Numerical Techniques for Cavitation Erosion Prediction*, Springer, 2014, pp. 123-163.

[23] "Boundary Element Method Module, 3DynaFS-BEM," [Online]. Available: http://www.dynaflow-inc.com/Products/Software/2_3DynaFS/Boundary-Element-3DynaFS.htm. [Accessed June 2021].

[24] J.-P. Franc and J.-M. Michel, "Cavitation Erosion," in *Fundamentals of Cavitation*, Kluwer Academic Publishers, 2005, pp. 265-291.

[25] A. Karimi and W. R. Leo, "Phenomenological Model for Cavitation Erosion Aggressiveness," in *Materials Science and Engineering*, Lausanne, Switzerland, 1987, pp. 1-14.

[26] J. Steller and B. G. Gireń, International Cavitation Erosion Test - Final Report, Gdańsk: Instytut Maszyn Przepływowych im. Roberta Szewalskiego Polskiej Akademii Nauk, 2015.

[27] E. O. Aidoo, "Material response on the cavitation bubble collapses (Master thesis)," Technical University of Liberec, Liberec, Czech Republic, 2018.

[28] B. G. Gireń and J. Frączak, "Phenomenological prediction tool for cavitation erosion fed with the International Cavitation Erosion Test results," *Wear,* Vols. 364-365, pp. 1-9, 2016.

[29] J. Styková, M. Müller and J. Hujer, "The improvement of the surface hardness of stainless steel and aluminium alloy by ultrasonic cavitation peening," in *EPJ Web of Conferences 143, EFM16 - Experimental Fluid Mechanics*, Mariánské Lázně, Czech Republic, 2016.

[30] F. T. Huluka, "Application of nano-layers for the improvement of the cavitation resistance (Master thesis)," Technical University of Liberec, Liberec, Czech Republic, 2020.

[31] "UIP1000hdT – Powerful and Versatile Homogenizer," Hielscher, [Online]. Available: https://www.hielscher.com/i1000_p.htm. [Accessed April 2021].

[32] "ALUNET hliníkové profily na míru," [Online]. Available: http://www.alunet.cz/ENAW-7075. [Accessed May 2021].

[33] Measurement Specialties, Inc., *Piezo Film Sensors: Technical Manual,* Measurement Specialties, Incorporated, 1999.

[34] SMLease Design, "Stress Strain Curve: Strength of Materials," [Online]. Available: https://www.smlease.com/entries/mechanical-design-basics/stress-strain-curve-diagram/. [Accessed 2 June 2021].

[35] J. R. da Cruz, S. L. Henke and A. S. d'Oliveira, "Effect of Cold Work on Cavitation Resistance of an Austenitic Stainless Steel," *Materials Research,* p. 10, August 2016.

[36] K. Peng, S. Tian, G. Li, Z. Huang, R. Yang and Z. Guo, "Bubble dynamics characteristics and influencing factors on the cavitation collapse intensity for self-resonating cavitating jets," *Petroleum Exploration and Development,* pp. 343-350, 2018.

[37] "The Process Piping," [Online]. Available: https://www.theprocesspiping.com/introduction-to-cavitation/. [Accessed January 2021].